Semi-annual Informal Progress Report

submitted to

National Aeronautics and Space Administration-Johnson Space Center

Technical Officer: K. M. Hurlbert
EC3/34546
NASA-JSC, Houston, Texas 77058

Grant ID # NAG 9-854

Title: Heat and Momentum Transfer Studies in High Reynolds Number Wavy Films at Normal and Reduced Gravity Conditions

P.I: V. Balakotaiah
Department of Chemical Engineering
University of Houston
Houston, Texas 77204-4792

February 26,1996

Administrative Notes:

The grant funds were released only on November 1,1995 with back dating of the grant to August 1,1995. A new graduate student (Mr. Luan Nguyen) could be appointed on the grant only on January 2, 1996. The work reported here was done by the PI and a former graduate student. It will be continued by the PI and the new graduate student for the remaining duration of the project.

Technical Progress - Summary :

Work Completed:

In our earlier work, we developed mathematical models that can describe the behavior of free falling wavy films at high Reynolds numbers. One major objective of our proposed work was to extend these models to include the co or counter-current flow of gas. In the first phase of our work, we have completed the extension and analysis of the model for counter-current gas flow. The details of the model and the analysis are given in the Appendix to this report. We are presently in the process of writing up the results of this study as a publication in a refereed journal.

Work to be Completed:

The PI and the new graduate student are now working on the extension of the boundary layer models to microgravity conditions. We hope to complete this extension as well as obtain some theoretical results that may be used to compare with experimental data. We also plan to complete the study of heat (and mass) transfer enhancement studies in wavy films at high Reynolds numbers. The results of these two extensions will be reported in the final report.

Semi-annual Progress Report:

Grant # NAG 9-854:

Heat and Momentum Transfer Studies in High Reynolds Number Wavy Films at Normal and Reduced Gravity Conditions

1. Introduction:

The most dramatic effect of the simultaneous flow of gas and liquid in pipes is the greatly increased transport rates of heat, mass and momentum. In practical situations this enhancement can be a benefit or it can result in serious operational problems. For example, gas-liquid flow always results in substantially higher pressure drop and this is usually undesirable. However, much higher heat transfer coefficients can be expected and this can obviously be of benefit for purposes of design. Unfortunately, designers know so little of the behavior of such two phase systems and as a result these advantages are not utilized. In the first phase of our work, we examined the effect of the gas flow on the liquid film when the gas flows in the countercurrent direction in a vertical pipe at normal gravity conditions.

Only a few theoretical studies dealt with wavy motion with countercurrent or cocurrent gas flow. Kapitza [1] studied the effect of countercurrent or cocurrent gas flow in the momentum equation for the interfacial shear stress, which arises from the gas-liquid interaction. The most significant contribution to wave modeling for horizontal gas-liquid flow in thin film has been presented by Miya et al.[2]. A solitary wave was considered and a shock condition at the wave front was utilized. This model satisfactorily predicts the interfacial shape, wall shear stress, pressure drop, and other wave variables. The approach is still rather approximate since experimental data is needed as an input to provide a solution. Brauner et al.[3] used an integral approach to model waves observed in cocurrent downward annular gas-liquid flow.

The experimental studies of countercurrent flow have been made by many researchers. Important parameters for the description of countercurrent flow are pressure drop, wall shear

stress and interfacial wave structure. Pressure drop measurements have been made by Feind[4] , Dukler and Smith [5], and Zabaras[6]. For adiabatic flow, the pressure drop slowly increases before the flooding point as the gas rate is increased under constant liquid rate. Most studies of interfacial wave structure have been restricted in measurements of the time average film thickness (Feind[4], Dukler and Smith[5]). The results of these investigators show that the mean film thickness is not significantly affected by the upward flow of the gas, although no quantitative expressions were presented. Experimental results indicate that the mean film thickness with countercurrent gas flow increases by approximately 10% to 20% over the film thicknesses with zero gas flow. Wave frequencies and wave velocities in vertical countercurrent flow are given by Hewitt and Wallis [7] and Zabaras [6]. These investigators report that there is little influence of the countercurrent air flow on the wave velocities in falling films.

2. Model Formulation

We consider a viscous fluid film flowing down a vertical plate under gravity with a countercurrent stream of gas phase adjoining the free surface. The particular flow situation considered is one for which there is no exchange of droplets between the film and gas. We assume that the film thickness is considerably smaller than any length scale in the mean flow direction and all the variables are independent of the transverse coordinate. The two-dimensional Navier-Stokes equations for an incompressible fluid are

$$\frac{\partial \mathbf{u}}{\partial t} + \mathbf{u}\cdot\nabla\mathbf{u} = -\frac{1}{\rho}\nabla p + \mathbf{g} + \nu\nabla^2\mathbf{u}\,, \tag{2.1}$$

$$\nabla\cdot\mathbf{u} = 0\,, \tag{2.2}$$

where $\mathbf{u} = (u,v)$ is the velocity field, and $\mathbf{g} = (g, 0)$. The coordinate system is chosen such that the y direction is normal to the wall and x direction is aligned with gravity (Figure 1). The pressure in the gas phase is p_g, the kinematic and interface stress conditions can be written as

$$v(h) = u(h)\frac{\partial h}{\partial x} + \frac{\partial h}{\partial t} \quad @\ y = h(x,t)\,, \tag{2.3}$$

$$\left(\frac{\partial u}{\partial y}+\frac{\partial v}{\partial x}\right)\left(1-h_x^2\right)+2\left(\frac{\partial v}{\partial y}-\frac{\partial u}{\partial x}\right)h_x = b \quad @\ y = h(x,t)\,, \tag{2.4}$$

$$p-p_g+\mu\left(\frac{\partial u}{\partial y}+\frac{\partial v}{\partial x}\right)\frac{h_x}{1+h_x^2}-2\mu\frac{\partial u}{\partial x}\frac{h_x^2}{1+h_x^2}-2\mu\frac{\partial v}{\partial y}\frac{1}{1+h_x^2}+$$

$$\sigma\frac{h_{xx}}{\left(1+h_x^2\right)^{3/2}} = 0 \quad @\ y = h\ , \tag{2.5}$$

where

$$b = \frac{\tau_i}{\mu}\,,$$

and τ_i is the interfacial shear stress.

There is also the no-slip condition at the wall,

$$\mathbf{u} = 0 \qquad @\ y = 0\ . \tag{2.6}$$

For the gas phase, a shallow fluid assumption is made to simply the relation between p_g and film thickness h. The justification for this assumption for the gas flow is not so good as for the liquid film flow since the thickness of gas layer is much greater than the thickness of the liquid layer. Support for this assumption can be found elsewhere [2].

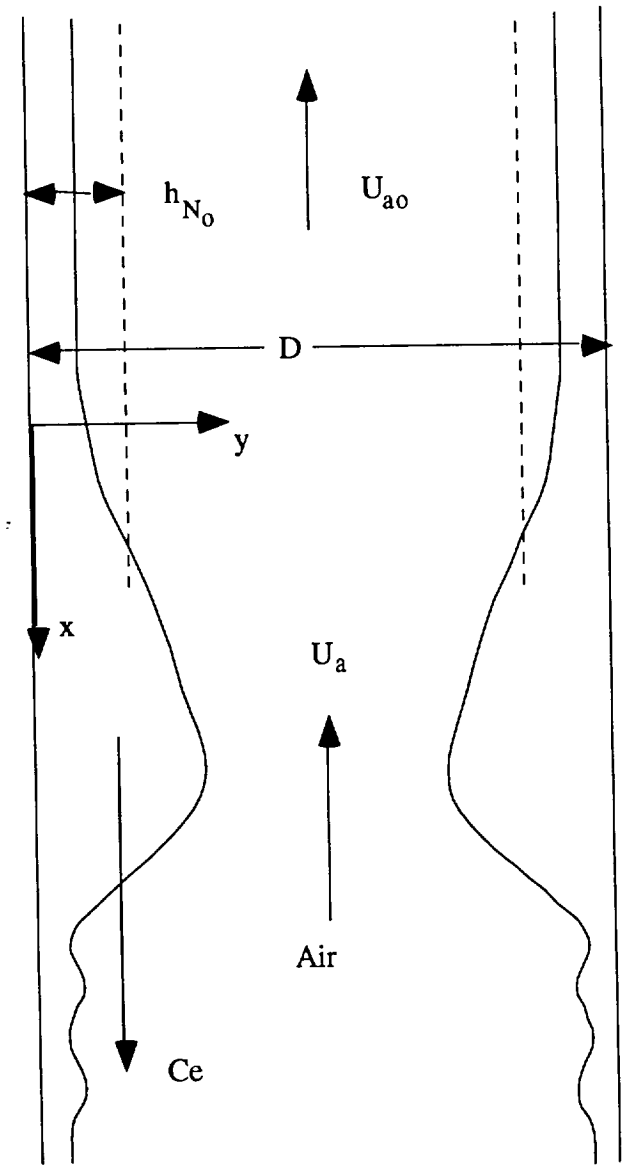

Figure 1: Schematic representation of countercurrent gas-liquid flow.

By using the shallow gas assumption, a momentum balance and mass balance can be developed for the gas phase. For the case of a countercurrent stream of gas phase adjoining the free surface, we have

$$\frac{d\left(\frac{\rho_g}{2}(U_a+V_w)^2\right)}{dx} = -\frac{2\tau_i}{D-2h} - \frac{dp_g}{dx} \qquad (2.7)$$

and

$$(D-2h)(U_a+V_w) = (D-2h_N)(U_{ao}+u_{Ni}) \ , \qquad (2.8)$$

where D is the diameter of the column, ρ_g, the gas density, U_a, the local average gas velocity and U_{ao}, the average gas velocity over the base film, V_w the wave velocity and u_{Ni} is the average velocity of the flat film. The interfacial shear stress is defined as

$$\tau_i = \frac{\rho_g}{2} f_s (U_a + V_w)^2 \ , \qquad (2.9)$$

where f_s is interfacial fraction factor.

Substituting equation (2.8) and (2.9) into equation (2.7) leads to

$$\frac{dp_g}{dx} = -\rho_g f_s \frac{(U_{ao}+u_{Ni})^2 (D-2h_N)^2}{(D-2h)^3} \left(1 + \frac{2}{f_s}\frac{\partial h}{\partial x}\right). \qquad (2.10)$$

The interfacial friction factor f_s can be obtained from the pressure drop measurements and it is a function of the liquid flow rate. Equations (2.1)-(2.10) define the full equations of motion for the annular countercurrent gas-liquid two-dimensional falling film problem. We will start our analysis by considering the simplified equations for steady, laminar, one-dimensional smooth film motion with the countercurrent air flow ,

$$\nu\frac{\partial^2 u}{\partial y^2} + g - \frac{1}{\rho}\frac{dp}{dx} = 0. \qquad (2.11)$$

BC's
$$u = 0 \qquad @ \quad y = 0\,, \tag{2.12}$$

$$\mu \frac{\partial u}{\partial y} = \tau_i \qquad @ \quad y = h\,, \tag{2.13}$$

where τ_i represents the interfacial shear stress.

The solution of equation (2.11) yields the following velocity distribution,

$$u_o(y) = \frac{\phi h}{\nu}\left(\left(1+\frac{\tau_i}{\rho\phi h}\right)y - \frac{y^2}{2h}\right), \tag{2.14}$$

where

$$\phi = g - \frac{1}{\rho}\frac{dp}{dx}\,. \tag{2.15}$$

It follows from equation (2.14) that the average velocity of the flat film is given by

$$u_{Ni} = \frac{\phi h^2}{3\nu} + \frac{\tau_i\, h}{2\mu}\,. \tag{2.17}$$

In order to simplify the two-dimensional model equations, we use a boundary layer type analysis. We scale the streamwise coordinate x by the unknown wavelength λ, the normal coordinate y by h_N (Nusselt film thickness without any interfacial shear), the x-component of velocity by u_N (average Nusselt velocity), the y-component of velocity by εu_N (where $\varepsilon = h_N/\lambda$), pressure by ρu_N^2 and time by λu_N. The scaled equations of motion and boundary conditions are

$$\frac{\partial u}{\partial t} + u\frac{\partial u}{\partial x} + v\frac{\partial u}{\partial y} = -\frac{\partial P}{\partial x} + \frac{12}{R} + \frac{4}{R}\left(\frac{\partial^2 u}{\partial y^2} + \varepsilon^2\frac{\partial^2 u}{\partial x^2}\right), \tag{2.18}$$

$$\varepsilon^2\left(\frac{\partial v}{\partial t} + u\frac{\partial v}{\partial x} + v\frac{\partial v}{\partial y}\right) = -\frac{\partial P}{\partial y} + \frac{4}{R}\left(\varepsilon^4\frac{\partial^2 v}{\partial x^2} + \varepsilon^2\frac{\partial^2 v}{\partial y^2}\right), \tag{2.19}$$

$$\frac{\partial u}{\partial x} + \frac{\partial v}{\partial y} = 0\,, \tag{2.20}$$

$$y = 0 \;; \qquad u = v = 0\,, \tag{2.21}$$

$$y = h(x,t) \quad ; \qquad v = h_t + u\, h_x \,. \tag{2.22}$$

The tangential stress condition at y = h(x,t) becomes

$$\left(\frac{\partial u}{\partial y} + \varepsilon^2\frac{\partial v}{\partial x}\right)\left(1 - \varepsilon^2 h_x^2\right) + 2\,\varepsilon^2\left(\frac{\partial v}{\partial y} - \frac{\partial u}{\partial x}\right)h_x = B \tag{2.23}$$

and the normal stress condition at y = h(x,t) is

$$P - P_g + \frac{8\varepsilon^2}{R}\left(\frac{\partial u}{\partial y} + \varepsilon^2\frac{\partial v}{\partial x}\right)\frac{h_x}{1+\varepsilon^2 h_x^2} - \frac{8\varepsilon^4}{R}\frac{\partial u}{\partial x}\frac{h_x^2}{1+\varepsilon^2 h_x^2} - \frac{8\varepsilon^2}{R}\frac{\partial v}{\partial y}\frac{1}{1+\varepsilon^2 h_x^2}$$

$$+\varepsilon^2 We\,\frac{h_{xx}}{\left(1+\varepsilon^2 h_x^2\right)^{3/2}} = 0\,, \tag{2.24}$$

where

$$R = \varepsilon Re, \tag{2.25}$$

$$B = \frac{h_N \tau_i}{u_N \mu}\,. \tag{2.26}$$

We now consider simplification of the above model valid for large Reynolds numbers. For $\varepsilon << 1$, $Re >> 1$, $\varepsilon Re = R = O(1)$ and $We = O(1/\varepsilon)$ (valid for high surface tension fluids such as water) the model may be simplified by dropping the terms that are of order ε^2 or higher. This leads to the extended form of the boundary layer model that is applicable in the presence of interfacial shear (in dimensional form):

$$\frac{Du}{Dt} = -\frac{1}{\rho}\frac{dp}{dx} + g + \nu\frac{\partial^2 u}{\partial y^2}\,, \tag{2.27}$$

$$\frac{dp}{dy} = 0\,, \tag{2.28}$$

$$\frac{\partial u}{\partial x} + \frac{\partial v}{\partial y} = 0\,, \tag{2.29}$$

$$u = v = 0 \qquad @\ y = 0\,, \tag{2.30}$$

$$\frac{\partial u}{\partial y} = \frac{\tau_i}{\mu} \qquad @\ y = h\,, \qquad (2.31)$$

$$\frac{dp}{dx} = -\,\sigma\, h_{xxx} + \frac{dp_g}{dx} \qquad @\ y = h, \qquad (2.32)$$

$$v = h_t + u\, h_x \qquad @\ y = h, \qquad (2.33)$$

$$\frac{dp_g}{dx} = -\,\rho_g f_s \frac{(U_{ao} + u_{Ni})^2\,(D - 2h_N)^2}{(D - 2h)^3}\left(1 + \frac{2}{f_s}\frac{\partial h}{\partial x}\right), \qquad (2.34)$$

$$\tau_i = \frac{\rho_g}{2} f_s \frac{(U_{ao} + u_{Ni})^2\,(D - 2h_N)^2}{(D - 2h)^2}\,. \qquad (2.35)$$

In this first approximation, the pressure is independent of y, the tangential stress condition is the same as that of the flat film and the normal stress condition includes surface tension and pressure gradient in the gas phase. In this paper we will only consider this boundary layer model. The second-order boundary layer model [8] will not be pursued because the pressure deviation across the film is negligible compared to the pressure applied on the interface because of the gas phase. The equations defining the boundary layer model are easier to deal with and expect this model to predict some observed wave characteristics as it includes all the leading order terms.

3. Method of Solution

We use the same formulation that can be found in Yu et al. [8]. to solve this problem, the only difference being in the tangential and normal stress boundary conditions. Because the flat film solution under the presence of tangential stress is different from that with zero shear stress, we need to find a different form of stream function that can deal with the flat film solution under the shear stress. We modify and write the stream function expansion as

$$\Psi(x,y,t) = a_2(x,t)\left(\left(1 + \frac{b}{2a_2}\right)y^2 - \frac{y^3}{3h}\right) + a_3(x,t)\left(y^3 - \frac{3y^4}{5h}\right) +$$

$$a_4(x,t)\left(y^4 - \frac{5y^5}{7h}\right) + a_5(x,t)\left(y^5 - \frac{7y^6}{9h}\right), \qquad (3.1)$$

where $b = \frac{\tau_i}{\mu}$.

The first term of this stream function is the flat film solution under the presence of shear stress. The rest of the terms are used as correction terms to the base solution in the presence of waves. The no slip boundary condition at the wall can be automatically satisfied by this streamfunction. We use the same integral and boundary collocation method that was used in Yu et. al. On the free surface, there exists a general continuity condition for the tangential shear stress (written in the form of streamfunction),

$$\left(\frac{\partial^2 \Psi}{\partial y^2}\right)_{y=h} = b. \tag{3.2}$$

Inserting the streamfunction expansion (1.3.1) into (1.3.2) results in the following equation,

$$175h^2 a_5 + 120a_4 h + 63a_3 = 0.$$

In this equation, a_5 is linear with respect to the other variables so we can solve for a_5 as

$$a_5 = -\frac{1}{175h^2}(120a_4 h + 63a_3). \tag{3.3}$$

After substituting for a_5 into (1.3.1), we can rewrite the streamfunction in the following form,

$$\Psi(x,y,t) = a_2(x,t)\left(\left(1 + \frac{b}{2a_2}\right)y^2 - \frac{y^3}{3h}\right) + a_3(x,t)\left(y^3 - \frac{3y^4}{5h}\right) + a_4(x,t)\left(y^4 - \frac{5y^5}{7h}\right)$$

$$- \frac{1}{175h^2}(120a_4(x,t)h + 63a_3(x,t))\left(y^5 - \frac{7y^6}{9h}\right). \tag{3.4}$$

The first condition used here is integral x-momentum equation to insure that the approximate velocity profile satisfies the global momentum balance for all times and locations. The x-momentum equation is integrated across the film,

$$\int_0^h \left(\frac{\partial u}{\partial t} + u \frac{\partial u}{\partial x} + v \frac{\partial u}{\partial y} + \frac{1}{\rho} \frac{dp}{dx} - g - \nu \left(\frac{\partial^2 u}{\partial y^2} \right) \right) dy = 0 . \qquad (3.5)$$

The result of integral x-momentum equation after simplification using Liebnitz' rule is

$$\frac{d}{dx} \int_0^h \left(\frac{\partial \Psi}{\partial y} \right)^2 dy + \frac{d}{dt} \left(\Psi(h(x,t)) \right) + \frac{h}{\rho} \frac{dp}{dx} - gh - \nu \int_0^h \frac{\partial^3 \Psi}{\partial y^3} dy = 0 . \qquad (3.6)$$

Inserting the streamfunction expansion (1.3.4) into (1.3.6), the resulting equation may be normalized with respect to the flat film solution. This procedure gives the following equation, which was obtained from a symbolic manipulation program (MACSYMA),

$$866250\, ReWeH \frac{\partial^3 H}{\partial X^3} + \{866250 \frac{dP_g}{dX} - [\, 62300\, A_4^2 H^6 + 221400\, A_3 A_4 H^5 +$$

$$(148500\, A_4 B + 297000 A_2 A_4 + 188937\, A_3^2) H^4 - (207900\, A_3 B + 465300\, A_2 A_3) H^3$$

$$+ (144375\, A_2 B + 231000\, A_2^2) H^2] \frac{\partial H}{\partial X} -$$

$$[\, 288750\, A_4 H^3 + 415800\, A_3 H^2 + 288750\, A_2 H] \frac{\partial H}{\partial T} -$$

$$21100\, A_4 H^7 \frac{\partial A_4}{\partial X} - 46140 (A_3 \frac{\partial A_4}{\partial X} + A_4 \frac{\partial A_3}{\partial X}) H^6$$

$$- (41250 \frac{\partial A_4}{\partial X} B + 82500\, A_2 \frac{\partial A_4}{\partial X} + 82500 \frac{\partial A_2}{\partial X} A_4 + 102186\, A_3 \frac{\partial A_3}{\partial X}) H^5$$

$$- (86625 \frac{\partial A_3}{\partial X} B + 115500 \frac{\partial A_4}{\partial T} + 185625\, A_2 \frac{\partial A_3}{\partial X} + 185625 \frac{\partial A_2}{\partial X} A_3) H^4$$

$$- (144375 \frac{\partial A_2}{\partial X} B + 277200 \frac{\partial A_3}{\partial T} + 346500\, A_2 \frac{\partial A_2}{\partial X}) H^3 + 577500 \frac{\partial A_2}{\partial T} H^2 \} Re$$

$$+10395000\, H - 6930000\, A_2 = 0. \qquad (3.7)$$

In this equation, the normalized pressure in the gas phase and interfacial shear stress can be expressed as

$$\frac{dP_g}{dX} = -\frac{\rho_g}{\rho_l} f_s \frac{(U+Ce)^2 (1-2\alpha)^2}{(1-2\alpha H)^3} \alpha \left(1 + \frac{2}{f_s} \frac{\partial H}{\partial X}\right), \qquad (3.8)$$

$$B = \frac{Re}{8} \frac{\rho_g}{\rho_l} f_s \frac{(U+Ce)^2 (1-2\alpha)^2}{(1-2\alpha H)^2}, \qquad (3.9)$$

where

$$U = \frac{U_{ao}}{u_N}, \qquad (3.10)$$

$$\alpha = \frac{h_N}{D}, (\alpha << 1) \qquad (3.11)$$

$$H = \frac{h}{h_N}. \qquad (3.12)$$

For the problem considered here, D is 50.8 mm and h_N is less than 0.5 mm when Re < 1500, so α is very small. For the range of values of H considered here($0 < H < 3$), αH is less than 0.03. Using the approximation,

$$\frac{1}{(1-a)^n} \approx 1 + na, \quad |a| << 1,$$

we can simplify equations (3.8) and (3.9) to

$$\frac{dP_g}{dX} = -m\alpha (1 + 6\alpha H)\left(1 + \frac{2}{f_s} \frac{\partial H}{\partial X}\right), \qquad (3.13)$$

$$B = \frac{Re}{8} m (1 + 4\alpha H), \qquad (3.14)$$

where

$$m = \frac{\rho_g}{\rho_l} f_s (U+Ce)^2 (1-2\alpha)^2. \qquad (3..15)$$

Taking the cross derivatives of the x and y momentum equations, equating like terms and evaluating near the wall leads to

$$\left(\frac{\partial^3\Psi}{\partial y^2\partial t} - \nu\left(2\frac{\partial^4\Psi}{\partial y^2\partial x^2} + \frac{\partial^4\Psi}{\partial y^4}\right)\right)_{y=0} = 0. \qquad (3.16)$$

Inserting (3.4) into (3.8) results in the following equation (in dimensionless form),

$$5\mathrm{Re}\frac{\partial A_2}{\partial T} - 40\frac{\partial^2 A_2}{\partial X^2} + 144\frac{A_3}{H} - 240A_4 = 0. \qquad (3.17)$$

The other collocation point we chose is at the interface, y = h. The x-momentum equation is evaluated at the interface (or infinitesimally close). At this position, the pressure gradient is specified by the capillary forces. The resulting partial differential equation, in term of the streamfunction, is

$$\left(\frac{\partial^2\Psi}{\partial y\partial t} + \frac{\partial^2\Psi}{\partial y\partial x}\frac{\partial\Psi}{\partial y} - \frac{\partial^2\Psi}{\partial y^2}\frac{\partial\Psi}{\partial x} + \frac{1}{\rho}\frac{dp}{dx} - g - \nu\frac{\partial^3\Psi}{\partial y^3}\right)_{y=h} = 0. \qquad (3.18)$$

Inserting the streamfunction expansion (3.3) into (3.18), the resulting equation was normalized with respect to the Nusselt flat film solution; it produces the following equation,

$$1875\,\mathrm{ReWeH}\frac{\partial^3 H}{\partial X^3} + \{1875\frac{dP_g}{dX} - [225A_4^2H^6 + 900A_3A_4H^5 - (500A_4B + 1500A_2A_4 + 864A_3^2)H^4 - 900(A_3B + 3A_2A_3)H^3 - (1250A_2B + 1875A_2^2)H^2)]\frac{\partial H}{\partial X}$$

$$- (1125A_4H^3 + 1800A_3H^2 + 1875A_2H)\frac{\partial H}{\partial X} - 75A_4H^7\frac{\partial A_4}{\partial X} -$$

$$180(A_3\frac{\partial A_4}{\partial X} - A_4\frac{\partial A_3}{\partial X})H^6 - (125B\frac{\partial A_4}{\partial X} + 375A_2\frac{\partial A_4}{\partial X} + 375\frac{\partial A_2}{\partial X}A_4$$

$$+ 432A_3\frac{\partial A_3}{\partial X})H^5 - 300(\frac{\partial A_3}{\partial X}B + \frac{5}{4}\frac{\partial A_4}{\partial T} + A_2\frac{\partial A_3}{\partial X} + 3A_3\frac{\partial A_2}{\partial X})H^4$$

$$- [625\frac{\partial A_2}{\partial X}B + 900\frac{\partial A_3}{\partial T} + 1875A_2\frac{\partial A_2}{\partial X} + (\frac{1875}{2}B + 1875A_2)\frac{dB}{dX}]H^3$$

$$- 1875\frac{\partial A_2}{\partial T}H^2\}\,\mathrm{Re} + 30000A_4H^2 + (27000A_3 + 22500)H - 15000A_2 = 0. \qquad (3.19)$$

The continuity relation,

$$\frac{\partial u}{\partial x} + \frac{\partial v}{\partial y} = 0 ,$$

is integrated across the film thickness, then using the Liebnitz' rule, the equation may be simplified and becomes

$$v(h) - v(0) - u(h) \frac{\partial h}{\partial x} + \frac{d}{dx} \int_0^h u dy = 0. \qquad (3.20)$$

At the free interface, the velocities are related through the kinematic condition,

$$v(h) = u(h) \frac{\partial h}{\partial x} + \frac{\partial h}{\partial t} . \qquad (3.21)$$

Substituting (3.20) into (3.21) and $V(0) = 0$ leads to

$$\frac{\partial h}{\partial t} + \frac{d}{dx} \int_0^h u dy =$$

$$\frac{\partial h}{\partial t} + \frac{d\Psi(h)}{dx} = 0 . \qquad (3.22)$$

When the streamfunction expansion (3.3) is inserted into (3.22), (3.22) becomes

$$\left(\frac{8}{15} A_4 H^3 + \frac{72}{75} A_3 H^2 + (B + \frac{4}{3} A_2) H \right) \frac{\partial H}{\partial X} + \frac{\partial H}{\partial T} +$$

$$\frac{2}{15} \frac{\partial A_4}{\partial X} H^4 + \frac{8}{25} \frac{\partial A_3}{\partial X} H^3 + \frac{2}{3} \frac{\partial A_2}{\partial X} H^2 = 0. \qquad (3.23)$$

The set of equations (3.7), (3.17), (3.19) and (3.23) can be solved for the unknown dimensionless variables A_2, A_3, A_4 and H as functions of position and time.

The steady state solution of this set of four equations can be obtained by letting all the derivative be zero. This gives the algebraic equation,

$$H_{ss}^3 - \frac{B}{2} H_{ss}^2 - 1 = 0, \qquad (3.24)$$

where B is a constant and H_{ss} is the dimensionless film thickness. Differentiating this equation with respect to H produces

$$H(3H - B) = 0,$$

$$H = 0, \text{ or } H = \frac{B}{3}.$$

If B is negative, there is only one positive solution, if B is positive, there are two positive solutions. The solution of the cubic equation (3.24) for $B < 0$ is shown in Figure 2. From this figure, we see that, when the shear stress increases, the film thickness will also increase .

4. Traveling Wave Model Formulation

As discussed earlier, the wave reaches an asymptotic steady state after traveling several hundred film thicknesses. We are more concerned the fully developed waves than the linear growth wave region. So the traveling wave formulation will be used.

Defining

$$Z = X - Ce\, T, \tag{4.1}$$

where X, Ce, and T are as defined x/h_N, c/u_N and t/u_N, motion with respect to the Z coordinate is steady, or

$$\frac{d}{dZ} = \left(\frac{\partial X}{\partial Z}\right)_T \frac{\partial}{\partial X} + \left(\frac{\partial T}{\partial Z}\right)_T \frac{\partial}{\partial T} = 0, \tag{4.2}$$

which allows the spatial and time derivatives to be written as

$$\frac{\partial}{\partial X} = \frac{d}{dZ} \tag{4.3}$$

and

$$\frac{\partial}{\partial T} = -Ce \frac{d}{dZ}. \tag{4.4}$$

The integral mass balance equation (3.23) in the traveling coordinate assumes the form of an exact differential,

$$\frac{d}{dZ}\left(\frac{2}{15}A_4 H^4+\frac{8}{25}A_3H^3+\frac{2}{3}\left(\frac{B}{2}+A_2\right)H^2 - Ce\, H\right)=0, \qquad (4.5)$$

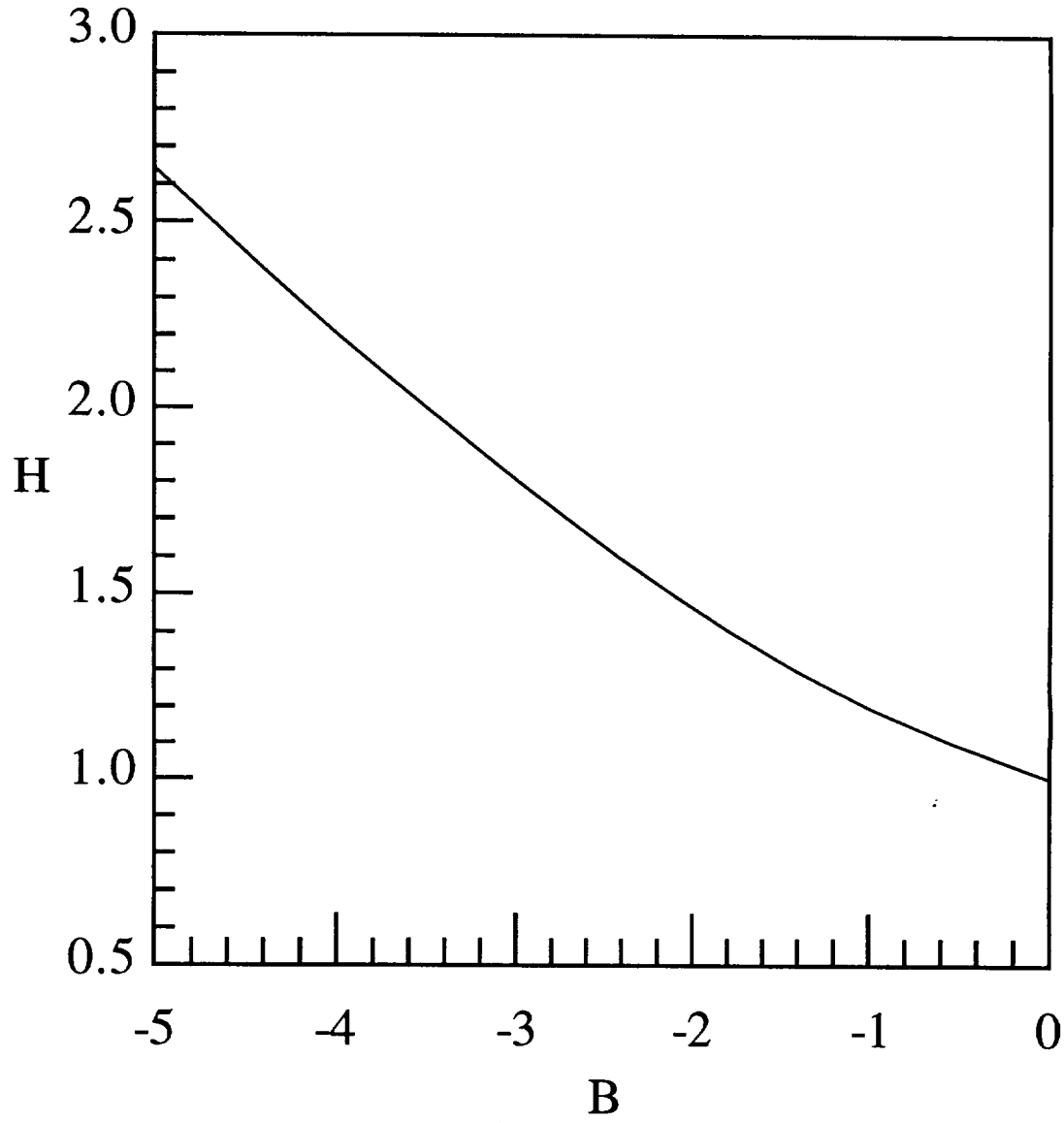

Figure 2 Film thickness steady state solution for different values of normalized interfacial shear.

or

$$\frac{d}{dZ}\left(\Psi(H) - Ce\,H\right) = 0. \tag{3.3}$$

For the flat film, there is a relation,

$$\Psi(H) - Ce\,H = 1 - Ce. \tag{4.5}$$

Substituting the streamfunction expansion (3.4) into above equation, the integral mass balance is used to solve directly for A_4,

$$A_4 = -\frac{1}{20H^4}\left(48A_3H^3+(75B+100A_2)H^2+150(Ce-CeH-1)\right). \tag{3.4}$$

Upon substitution of (7.3.4) into (3.7), (3.17) and (3.19) and transforming them to the traveling wave coordinate system produces the following equations:

$$\left(\frac{dB}{dZ} + 2\frac{dA_2}{dZ}\right)Ce\,H^4\,Re + 8\left(\frac{d^2B}{dZ^2} + 2\frac{d^2A_2}{dZ^2}\right)H^4 - 288\,A_3\,H^3 - 360\left(B + \frac{3}{2}A_2\right)H^2$$

$$+ 720\,(Ce\,H - Ce + 1) = 0, \tag{3.5}$$

$$16\,ReWeH^3\frac{d^3H}{dZ^3} + [16\,H^3\,\frac{dP_g}{dZ} + (-B^2H^4 - 2\,B\,Ce\,H^3 + 12\,(1 - Ce)\,CeH + 36Ce^2 -$$

$$72\,Ce + 36)\frac{dH}{dZ} - B\,\frac{dB}{dZ}H^5 - 2\,\frac{dB}{dZ}Ce\,H^4 + 6\,\frac{dB}{dZ}(Ce - 1)\,H\,]\,Re + 192(1 - 2A_3)\,H^3 -$$

$$(960\,B + 1408\,A_2)\,H^2 + 1920\,(Ce\,H - Ce + 1) = 0, \tag{3.6}$$

$$27720\,H^3\,Re\,We\frac{d^3H}{dZ^3} + \{27720\,H^3\,\frac{dP_g}{dZ} - [180\,A_3^2\,H^6 + (576\,A_3\,B + 1296\,A_2\,A_3)\,H^5$$

$$- (3240\,CeA_3 + 1125\,B + 2340\,BA_2 + 2352\,A_2)\,H^4 - ((4320\,B + 2160\,A_3 + 11040\,A_2)$$

$$Ce + 2160\,A_3)\,H^3 + (-12060\,Ce^2 + (-2160\,B - 5520\,A_2)\,Ce + 2160\,B + 5520\,A_2)\,H^2$$

$$+ 39780\,Ce^2 - 79560\,Ce + 39780]\,\frac{dH}{dZ} - 72\,A_3\,H^7\frac{dA_3}{dZ} - [\,144(A_3\frac{dB}{dZ} + B\frac{dA_3}{dZ}) +$$

$$324(\,A_2\frac{dA_3}{dZ} + A_3\frac{dA_3}{dZ})]\,H^6 + [1080Ce\,\frac{dA_3}{dZ} - (\,750\,B + 780\,A_2)\,\frac{dB}{dZ} - 780B\,\frac{dA_2}{dZ} -$$

$$1568\,A_2\,\frac{dA_2}{dZ}]\,H^5 + [(2160\,\frac{dB}{dZ} - 1080\,\frac{dA_3}{dZ} + 5520\,\frac{dA_2}{dZ})\,Ce + 1080\,\frac{dA_3}{dZ}]\,H^4$$

$$- [(\,2160\,\frac{dB}{dZ} + 5520\,\frac{dA_2}{dZ})\,Ce + 2160\,\frac{dB}{dZ} + 5520\,\frac{dA_2}{dZ}]\,H^3\,\}\,Re$$

$$+ 332640\,H^3 - 221760A_2H^2 = 0. \qquad (3.7)$$

These three equations may be written as a first order system by using MACSYMA to simplify and rearrange the expressions. The resulting system is written in the general form:

$$\frac{dH}{dZ} = \frac{d\theta_1}{dZ} = \theta_2\,, \qquad (3.8)$$

$$\frac{d^2H}{dZ^2} = \frac{d\theta_2}{dZ} = \theta_3\,, \qquad (3.9)$$

$$\frac{d^3H}{dZ^3} = \frac{d\theta_3}{dZ} = f_1(\underline{\theta}\,;\,Re,\,We,\,Ce), \qquad (3.10)$$

$$\frac{dA_2}{dZ} = \frac{d\theta_4}{dZ} = \theta_3\,, \qquad (3.11)$$

$$\frac{d^2A_2}{dZ^2} = \frac{d\theta_5}{dZ} = f_2(\underline{\theta}\,;\,Re,\,We,\,Ce), \qquad (3.12)$$

$$\frac{dA_3}{dZ} = \frac{d\theta_6}{dZ} = f_3(\underline{\theta}\,;\,Re,\,We,\,Ce)\,, \qquad (3.13)$$

where the dynamic variable vector is defined by

$$\theta = (\theta_1, \theta_2, \theta_3, \theta_4, \theta_5, \theta_6)^T = \left(H, \frac{dH}{dZ}, \frac{d^2H}{dZ^2}, A_2, \frac{dA_2}{dZ}, A_3\right)^T. \qquad (3.14)$$

The functions, which are autonomous (no Z dependence) and highly nonlinear are given below:

$$f_1(\underline{\theta}\,;\,Re,\,We,\,Ce) = -\frac{1}{16\theta_1{}^3ReWe}((16\theta_1{}^3P_Z+\theta_2(36Ce^2+12Ce\theta_1(1-Ce)-$$

$$2\theta_1{}^3BCe-72Ce-\theta_1{}^4B^2+36)+6\theta_1{}^3B_z(Ce-1)-2\theta_1{}^4B_ZCe-\theta_1{}^5BB_Z)Re+1920\,\theta_1Ce-$$

$$1920Ce+\theta_1{}^2(-960B-1408\theta_4)+\theta_1{}^3(192-384\theta_6)+1920), \qquad (3.15)$$

$$f_2(\underline{\theta}\,;\,Re,\,We,\,Ce) = -\frac{1}{16\theta_1{}^4}\,(\theta_1{}^4(B_Z+2\theta_5)CeRe+720\theta_1Ce-720Ce+8\theta_1{}^4\,B_{ZZ}$$

$$+\theta_1{}^2(-360B-480\theta_4)-288\theta_1{}^3\theta_6+720), \qquad (3.16)$$

$$f_3(\underline{\theta}\,;\,Re,\,We,\,Ce) = (27720\theta_1{}^3ReWef_1+(27720\theta_1{}^3P_Z+\theta_2(39780Ce^2+\theta_1{}^2(-12060Ce^2$$

$$+(-2160B-5520\theta_4)Ce+2160B+5520\theta_4)+\theta_1{}^3((4320B-2160\theta_6+11040\theta_4)Ce$$

$$+2160\theta_6)+\theta_1{}^4(3240\theta_6Ce-1125B^2-2340\theta_4B-2352\theta_4{}^2)-79560Ce+\theta_1{}^5(-576\theta_6B-1296\theta_4\theta_6)$$

$$-180\theta_1{}^6\theta_6{}^2+39780)+\theta_1{}^3((-2160\,B_Z-5520\theta_5)Ce+2160\,B_Z+5520\theta_5)+\theta_1{}^4(2160\,B_Z$$

$$+5520\theta(5))Ce+\theta_1{}^5((-750B-780\,\theta_4)\,B_Z-780\theta_5B-1568\theta_4\theta_5)$$

$$+\theta_1{}^6(-144\theta_6B_Z-324\theta_5\theta_6)Re-221760\theta_1{}^2\theta_4+332640\theta_1{}^3)/$$

$$((\theta_1{}^4(1080Ce-1080)1080\theta_1{}^5Ce+\theta_1{}^6(144B+324\theta_4)+72\theta_1{}^7\theta_6)Re), \qquad (3.17)$$

$$P_Z(Z) = -m\,\alpha\,(1+6\alpha\theta_1)(1+\frac{2}{f_s}\theta_2\,), \qquad (3.18)$$

$$B(Z) = M\,(1 + 4\alpha\theta_1)\,. \tag{3.19}$$

Steady state solutions are determined by the setting all derivatives with respect to Z to zero, and solving the resulting equations. This produces the steady state vector,

$$\underline{\theta}_{ss} = (\theta_{1ss}, 0, 0, \theta_{4ss}, 0, 0)^T, \tag{3.20}$$

where

$$\theta_{1ss} = H_{ss},$$

$$\theta_{4ss} = A_{2ss} = \frac{3}{2} H_{ss}\,.$$

A cubic polynomial for the steady state film thickness, H_{ss}, is obtained,

$$H_{ss}^3 + \frac{B}{2} H_{ss}^2 - Ce\,H_{ss} + Ce - 1 = 0\,, \tag{3.21}$$

where

$$B = \frac{Re}{8}\, m\,(1 + 4\alpha H_{ss})$$

$$= M\,(1 + 4\alpha H_{ss}) \tag{3.22}$$

$$\approx M\ (\text{constant}), \tag{3.23}$$

and $$M = \frac{Re}{8}\, m.$$

If $B = 0$, then equation (3.21) is same as that studied by Yu et al. [8] and there are two solutions,

$$H_{ss}^{(1)} = 1 \tag{3.24}$$

and

$$H_{ss}^{(2)} = -\frac{1}{2} + \sqrt{Ce - \frac{3}{4}}\,, \tag{3.25}$$

the first of which corresponds to flat film, and the second to another physical root existing for Ce $> \frac{3}{4}$ (which is from the transformation of the coordinate system). If $B \neq 0$, we let $D = \frac{B}{2}$, and rewrite the cubic equation as follows,

$$H_{ss}^3 + DH_{ss}^2 - Ce\, H_{ss} + Ce - 1 = 0. \qquad (3.26)$$

Depending on the values of Ce and D, this equation may have either zero, one, two or three feasible solutions for H_{ss}. First we note that when Ce = 1, the roots are given by

$$H_{ss} = 0,$$

$$H_{ss} = \frac{1}{2}\left(-D + \sqrt{D^2+4}\right). \qquad (3.27)$$

To determine the cusp point of equation (3.26) at which the three roots come together, we differentiate it with respect to H, once and twice and set the derivatives to zero. This gives

$$3H_{ss}^2 + 2DH_{ss} - Ce = 0 \qquad (3.28)$$

and

$$3H_{ss} + D = 0. \qquad (3.29)$$

Solving the three simultaneous equations (3.26), (3.28) and (3.29) gives the cusp point coordinates,

$$H_{ss} = \left(\frac{\sqrt{5}+3}{2}\right)^{1/3} + \left(\frac{\sqrt{5}+3}{2}\right)^{1/3} + 1 = 3.1,$$

$$Ce = \frac{H_{ss}^3 + 2}{2 - H_{ss}} = -28.9\ ,$$

$$D = \frac{(H_{ss}-1)^2(2H_{ss}+1)}{H_{ss}(2-H_{ss})} = -9.31.$$

The bifurcation set of equation (3.26) crossing which the number of solutions changes by two is obtained by solving equations (3.28) and (3.29) in a parametric form,

$$Ce = \frac{H_{ss}^3 + 2}{2 - H_{ss}}, \tag{3.30}$$

$$D = \frac{(H_{ss}-1)^2(2H_{ss}+1)}{H_{ss}(2 - H_{ss})}. \tag{3.31}$$

From these two expressions, we observe that

$$D \to \infty, \; Ce \to 1 \text{ as } H \to 0,$$

$$D = 0, \; Ce = 3 \text{ as } H \to 1,$$

$$D \to \infty, Ce \to \infty \text{ as } H \to 2.$$

We show in Figure 3 the different regions in the (Ce, D) plane in which equation (3.26) has zero, one, two and three solutions. We now consider each of these regions:

Region I: there are two film thicknesses for countercurrent or cocurrent gas flow (D positive or negative)

Region II: In this region, there is no positive solution to equation (3.26). The reason may be when the gas flow is countercurrent, the film may be pushed away and eventually no film exists.

Region III: In this region, Ce < 1 and there is only one positive film thickness for cocurrent or countercurrent gas flow.

Region IV: In this region, there are three positive solutions if gas flow is the countercurrent and very high, possibly beyond the flooding transition where there is liquid flow in both directions.

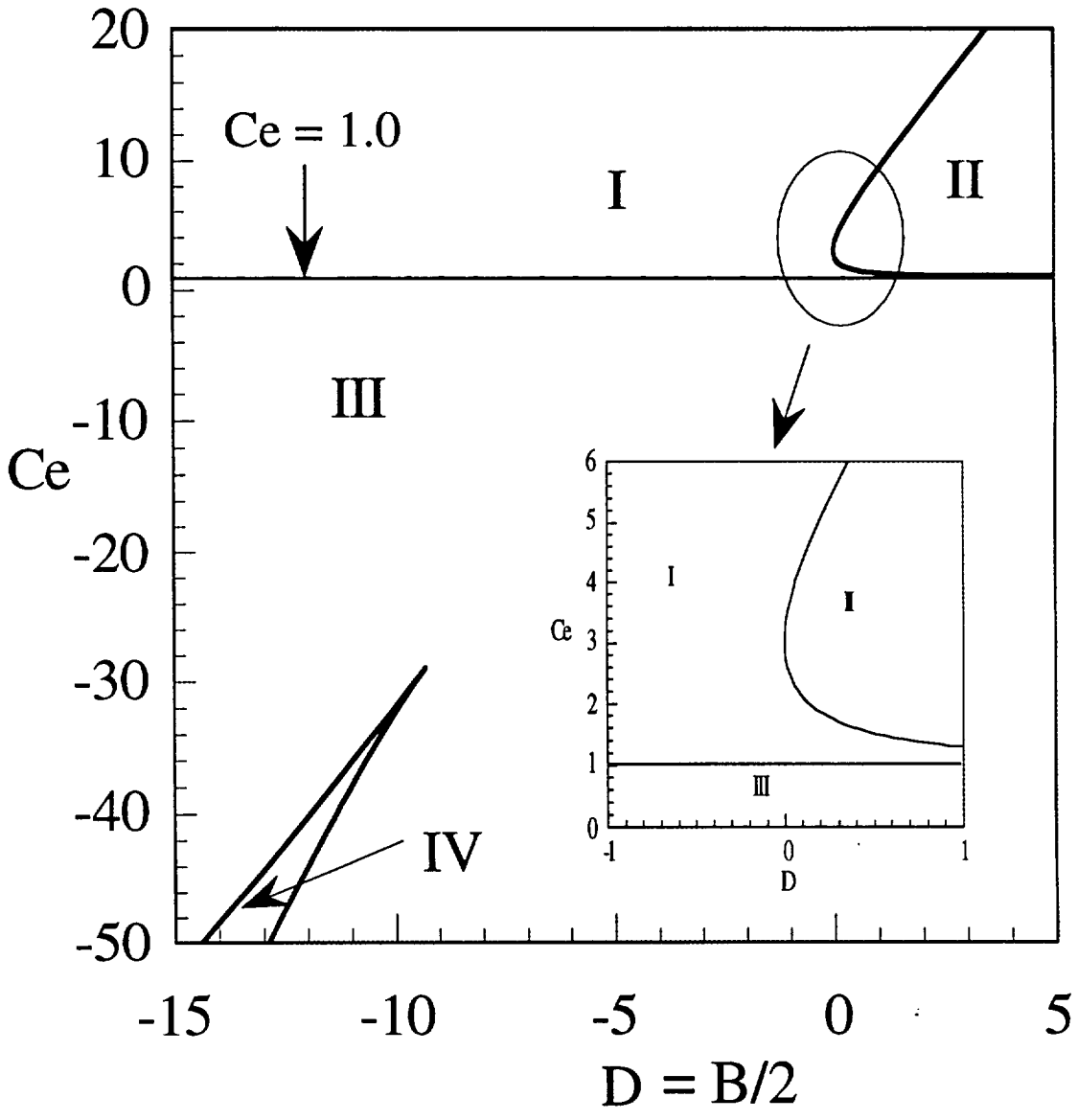

Figure 3 The Bifurcation diagram of film thickness solution in the Ce and D plane.

In this work, we consider countercurrent gas flow in region I, that is, B less than zero and Ce positive (before flooding), so there are two positive film thickness solutions. We plot the two

solutions of the cubic equation (3.24) in Figure 4 for different values of B. When B = 0, the two solution branches intersect at Ce = 3.0, but if B < 0, the two branch will separate and form isolated branches shown in Figure 7.4. When the value of B is increased, the top branch will go up and the lower branch will go down. We now investigate the linear stability of these two separated solution branches. We represent the two steady states for this system as

$$\underline{\theta}_{ss}^{(1)} = (H_{ss}^{(1)}, 0, 0, \frac{3}{2}H_{ss}^{(1)}, 0, 0), \tag{3.32}$$

$$\underline{\theta}_{ss}^{(2)} = (H_{ss}^{(2)}, 0, 0, \frac{3}{2}H_{ss}^{(2)}, 0, 0). \tag{3.33}$$

The characteristic equations that define the eigenvalues of these states are very lengthy and are not listed here. The polynomial equation was solved numerically for Re between 1 and 1200, Ce between 1.0 to 3.2 for a fixed value of the Kapitza number, Ka (Ka = 3371, water). For each value of Ka, the unstable manifold dimensions for both steady states as functions of Re and Ce was generated. Figure 5 shows the unstable manifold dimension for the steady state $H_{ss}^{(1)}$ at Ka = 3371. There is one Hopf line for the first steady state. The lower steady state ($H_{ss}^{(2)}$) is always unstable, that is, at least one real eigenvalue is positive. When Re is small, the Hopf line is very sensitive to the interfacial shear stress. When Re is increased, the celerity at the Hopf point is less sensitive. For the upper steady state film thickness $H_{ss}^{(1)}$, the Hopf line drops quickly and reaches an asymptotic value that depends on the shear stress value for Re values of 1200 or higher. For Ce greater than the Hopf celerity, the unstable manifold dimension is zero, meaning all small perturbations of the steady film are damped, and the film is linearly stable. Below the Hopf line, the unstable manifold dimension is 2, corresponding to a pair of eigenvalues crossing the imaginary axis. For the lower film thickness, the unstable manifold dimension is always great than one.

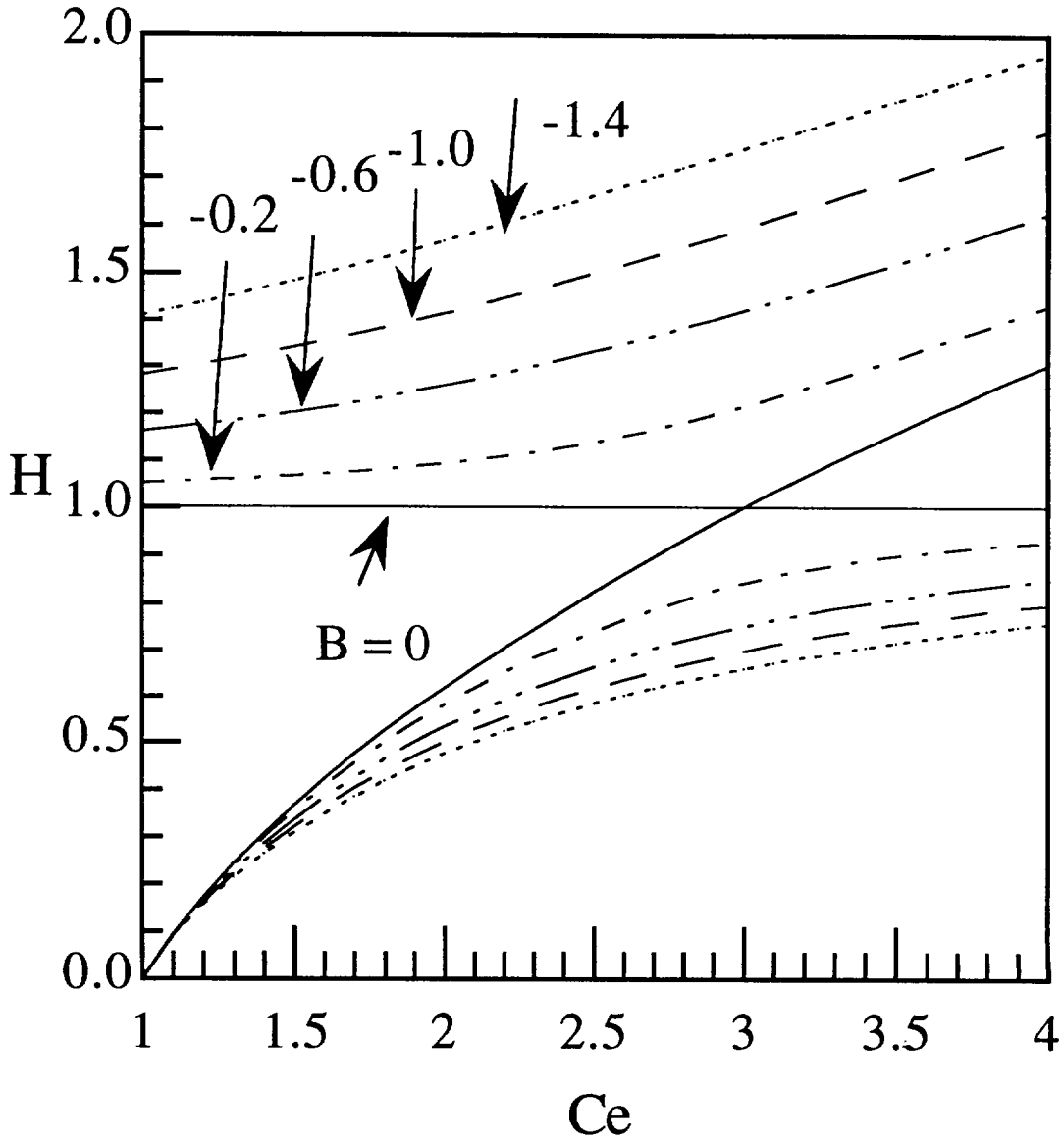

Figure 4: Steady state film thickness for different interfacial shear stress values.

The bifurcation diagram of the solutions shown in Figure 5 suggests all the interesting dynamic behavior occurs around the first flat film thickness. Additionally, the location of the wave inception line varies significantly with flowrate, agreeing with the experimental observations that fully developed films have different average wave velocities at different flowrates. The figure also shows that wave celerity is more sensitive to countercurrent gas flow for low liquid flowrates. The experimental data show that for liquid Reynolds number less than 400, the wave celerity increases with increasing gas flow, but for Reynolds number larger than that the wave celerity changes little until the flooding point is approached [6].

5. Numerical Study of the Traveling Wave Model Equations

The numerical method and analysis procedure used in this section are the same as those used in the last chapter. The aim of this study is to examine how the film profile character changes with varying wave celerities, Ce and shear stress B, for a fixed value of the Reynolds number and physical property group, Ka.

The numerical study includes three parts:

(1) determination of the capability of the model to produce statistically stationary wave forms and sensitivity to initial conditions,

(2) a study of the character of the stationary wave forms,

(3) a search for the values of Ce below which no bounded solutions exist. Integration of the system of ODEs required specification of initial conditions as well as a step size in the Z direction. Initial conditions were based on a perturbed flat film at the lower steady state thickness. In this study the film thickness was perturbed by 0.1% while all others retained their steady state values.

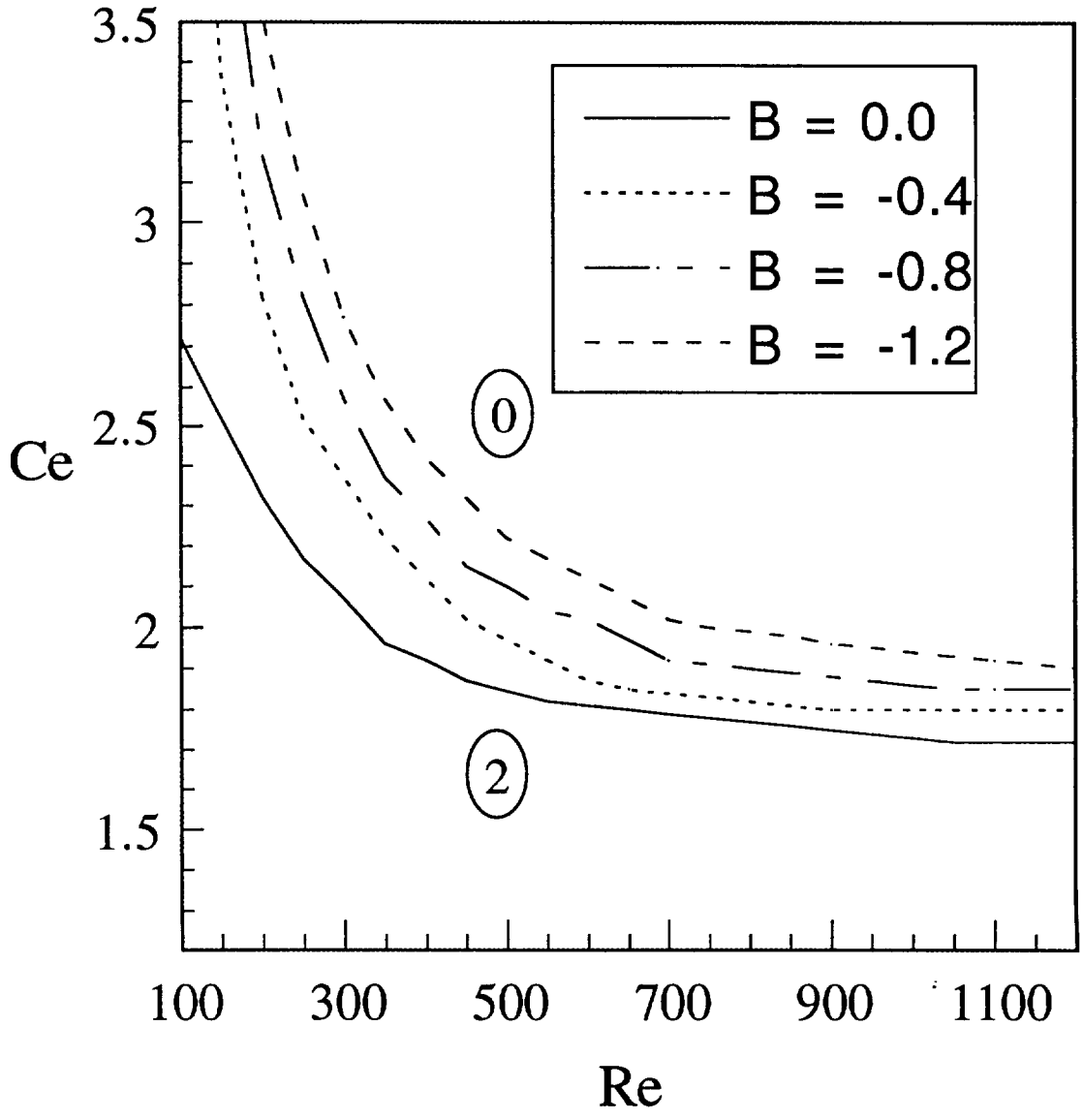

Fig. 5: Unstable manifold dimension map for Ka = 3371 at B = 0.0, B= 0.4, B= -0.8 and B= -1.2.

6. Sample Integration Results for Re = 600 and different values of interfacial shear stress

In this study we are more concerned with the shear stress effect on the liquid film. Therefore, we use one typical flowrate corresponding Re = 600 and different values of shear stress. The dimensionless shear stress B is defined as

$$B = M\,(1 + 4\alpha H), \tag{5.1}$$

where

$$M = \frac{mRe}{8}, \tag{5.2}$$

$$m = \frac{\rho_g}{\rho_l} f_s (U + Ce)^2\,(1 - 2\alpha)^2. \tag{3.15}$$

The expression for the pressure deviation in the gas phase is

$$\frac{dP_g}{dZ} = -\,m\,\alpha\,(1 + 6\alpha H)\left(1 + \frac{2}{f_s}\frac{\partial H}{\partial Z}\right). \tag{3.13}$$

Substituting (7.4.1) into (1.3.13) leads to

$$\frac{dP_g}{dZ} = -\,\frac{8M}{Re}\,\alpha\,(1 + 6\alpha H)\left(1 + \frac{2}{f_s}\frac{\partial H}{\partial Z}\right). \tag{5.3}$$

In (7.4.3), the only unknown is interfacial shear stress f_s which also appears in the expression for M. For the flowrate considered here, f_s is about 0.02 [2]. Because the value of B is not constant due to the wave present, a value of M is specified prior to each calculation. From expressions (4.1) and (4.3) the shear stress values in the normal and tangential direction are calculated and through expression (4.2) and (3.15) the dimensional gas velocity can be found to compare with the experimental data. For the flat film case, M is the same as B.

A series of values of M are used to study the gas-liquid interaction at the interface. The values of M are in the range zero to -1.5 and the gas velocity associated with these values is from zero to 30 m/s. This range covers most laminar falling film flows.

5.1 M = -0.2

The celerity at the Hopf point for Re = 600 is 1.88. For Ce slightly below this value, the wave profile is sinusoidal with a single frequency. When the celerity is reduced, the wave amplitude become larger and the periodicity is lost. The transition from periodic to chaotic profile is similar to that with zero gas flow. We present here the wave profile for the smallest celerity value 1.785 for which a bounded solution exist. As shown in Figure 6, the wave thickness is larger than that for the free falling film due to the interfacial shear. The smallest value of wave celerity (1.785) for which a bounded solution exist has increased from that of the free falling film (1.73805). The film thickness and film slope phase plane shows the largest peak to substrate is 3.2 and the wave is more symmetric because the interfacial shear stress is in opposite direction to the gravity force(Figure 7). The power spectra and probability function shows no significant changes (Figure 8) other than the PDF is spread around the mean film thickness. This means the upward gas flow does not affect the nature of the falling film significantly at this value of M.

.2 M = -1.0

The celerity at the Hopf point for Re = 600 is 2.2. At near the Hopf celerity, the wave profile is sinusoidal with a single frequency. When reducing the celerity value the wave amplitude become larger and the also lose the periodicity. These transition is similar with the zero gas flow. The results presented here is for the smallest celerity value 1.91 that has bounded solutions. The wave thickness is larger than the free falling film due to the shear stress affect(Figure 9). The wave celerity 1.84 is also increased from 1.84 (M= -0.6) due to the increasing of the film thickness. The film thickness and film slope phase plane (Figure 10) shows the peak to substrate ratio is 5.5 and the wave is more symmetry than before. The power spectra and probability function shows no significant changes (Figure 11).

M = -1.3

The celerity at the Hopf point for Re = 600 is 2.35. At near the Hopf celerity, the wave profile is sinusoidal with single frequency. When reducing the celerity value the waveamplitude become larger and the also lose the periodicity. These transition is similar with the zero gas flow. The

results presented here is for the smallest celerity value 1.97 that has bounded solutions. The wave thickness is larger than the free falling film due to the shear stress affect (Figure 12). The wave celerity 1.97 is also increased from 1.91 (M= -1.0) due to the increasing of the film thickness. The film thickness and film slope phase plane (Figure 13) shows the peak to substrate ratio is 6 and the wave is more symmetry than before. The power spectra shows no significant changes that means the gas flow does not affect the natural of the falling film flow and the center of probability function moves to the right direction (Figure 14). The PDF is also spreading along the film thickness and the gas flow increase the film randomness.

Streamline maps are generated for different shear stress values to study the effect of countercurrent gas flow. For M = -0.6 there is no significant difference in the streamlines compared with that of the zero stress case [8]. There are two stagnation points on the interface streamline and there is a recirculation region under the wave peak (Figure 15).

For M = -1.0, there is one recirculation region when the wave is not very large (Figure 16(top)) . But a second recirculation region appears just under the interface for large waves (Figure 16(bottom)). This second recirculation is due to the interfacial shear stress and accounts for the increase in the interfacial mass transfer rate.

For M = -1.3, there are two recirculation regions in the wave even with a peak to substrate ratio of 2.6 (top diagram of Figure 17). The size of the second recirculation region increases when the shear stress is increased while the size of the first recirculation region decreases (bottom diagram of Figure 17).

7. Conclusions

The models that developed for free falling film flow are extended to study the countercurrent gas-liquid falling film flow. Due to the complexity of the second order boundary model as well as the pressure variation across the film is small compared to the imposed gas phase pressure, the countercurrent gas flow affect was studied for the standard boundary layer model. A different stream fuction that can compencete the shear stress affect was developed and this strean function

also can predict periodic solution. The descritized model equations were transformed to a traveling wave coordinate system. A stablity analysis of these sets of equations showed the presence of a Hopf bifurcation for certain values of the traveling wave velocity and the shear stress. The Hopf celerity was increased due to the countercurrent shear. For low flowrate the increases of celerity are more than for the high flow rate, that was also observed from the experiments. Numerical integration of a traveling wave simplification of the model also predicts the existence of chaotic large amplitude, non-periodic waves as observed in the experiments. The film thickness was increased by the shear.

8. References

[1]. Kapitza, P. L. & Kapitza, S. P., "Wave flow in thin layers of a viscous fluid". *Zh. Exper. i Teor Fiz.* **19**, 105; also in Collected Papers of P. L. Kapitza Vol. II, Macmillan, New York (1964).

[2]. Miya, M., Woodmansee, D. E. & Hanratty, T. J. "A Model for Roll Waves in Gas-liquid Flow", *Chem. Eng. Sci.*, **26**, 1915 (1971).

[3]. Brauner, N., Moalem-Maron, D. & Zijl, W., "Interfacial collocation equations of thin liquid film: Stability analysis". *Chem. Eng. Sci.*, **42**, 2025 (1987).

[4]. Feind, K., "Flow Studies in the Case of Counter Flow of Spray Film and Gas in Vertical Pipes", *Ver. Deut. Ingr.*, Forschungsh, 481(1960).

[5]. Dukler, A. E. and Smith, L., "Two-phase Interactions in Counter-current Flow. Studies of the Flooding Mechanism", Annual Report Nov. 1975-Oct. 1977, United States Nuclear Regulatory Commission NUREG/CR-0617 (1977).

[6]. Zabaras, G. J., "Studies of vertical, annular gas-liquid flow", Ph.D. Dissertation, University of Houston (1985).

[7]. Hewitt, G. F. & Wallis, G. B., "Flooding and Associated Phenomena in Falling Film Flow in a Vertical Tube", UKAEA Report AERE-R4022, 1963.

[8]. L.-Q. Yu, F. K. Wasden, A. E. Dukler and V. Balakotaiah, " Nonlinear Evolution of Waves on Falling Films at High Reynolds Numbers", Physics of Fluids, 7, 1866- 1902 (1995).

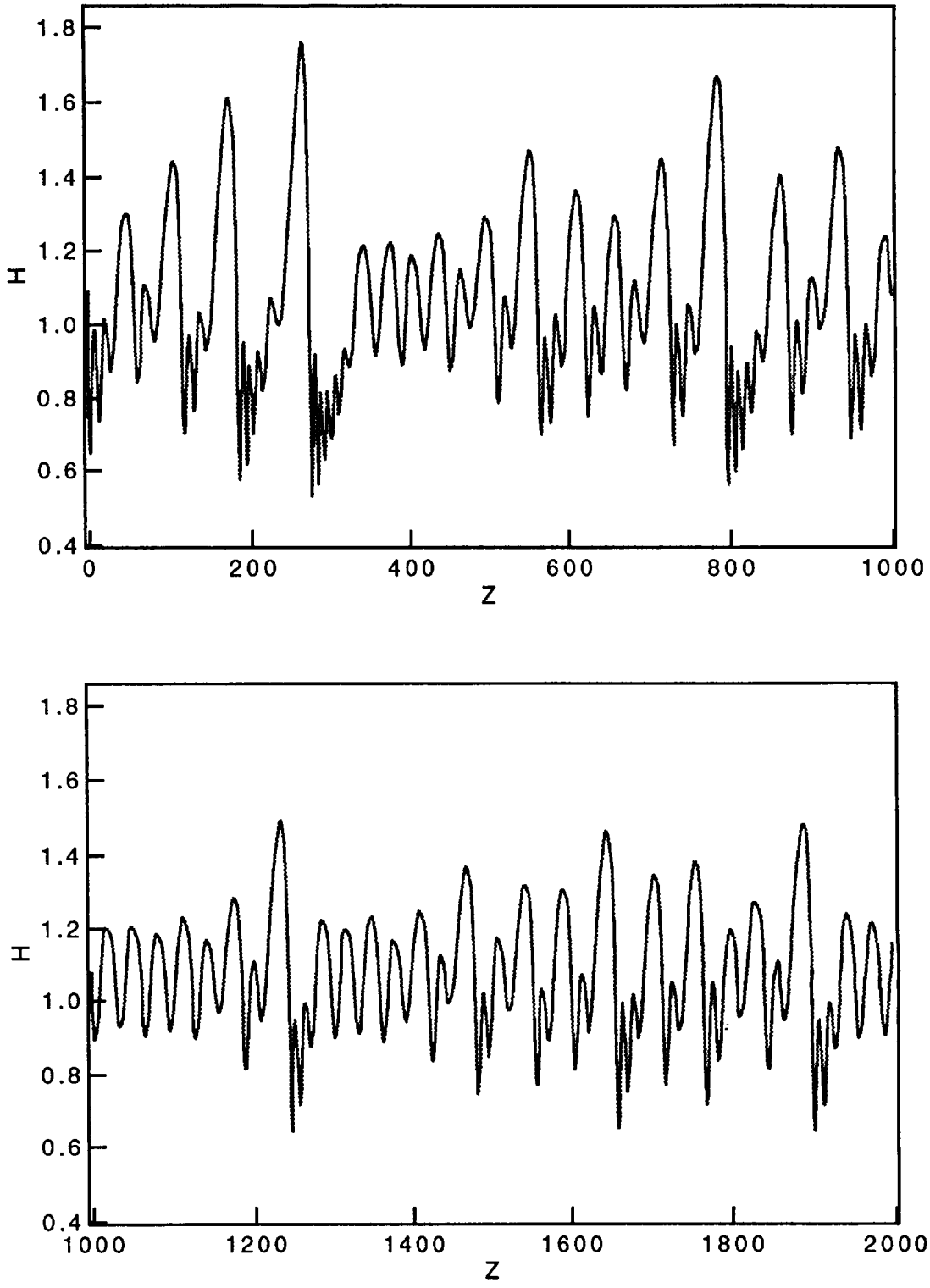

Figure 6: Normalized film thickness profile vs. distance for Re = 600, M = -0.2, Ce =1.785 and Ka = 3371.

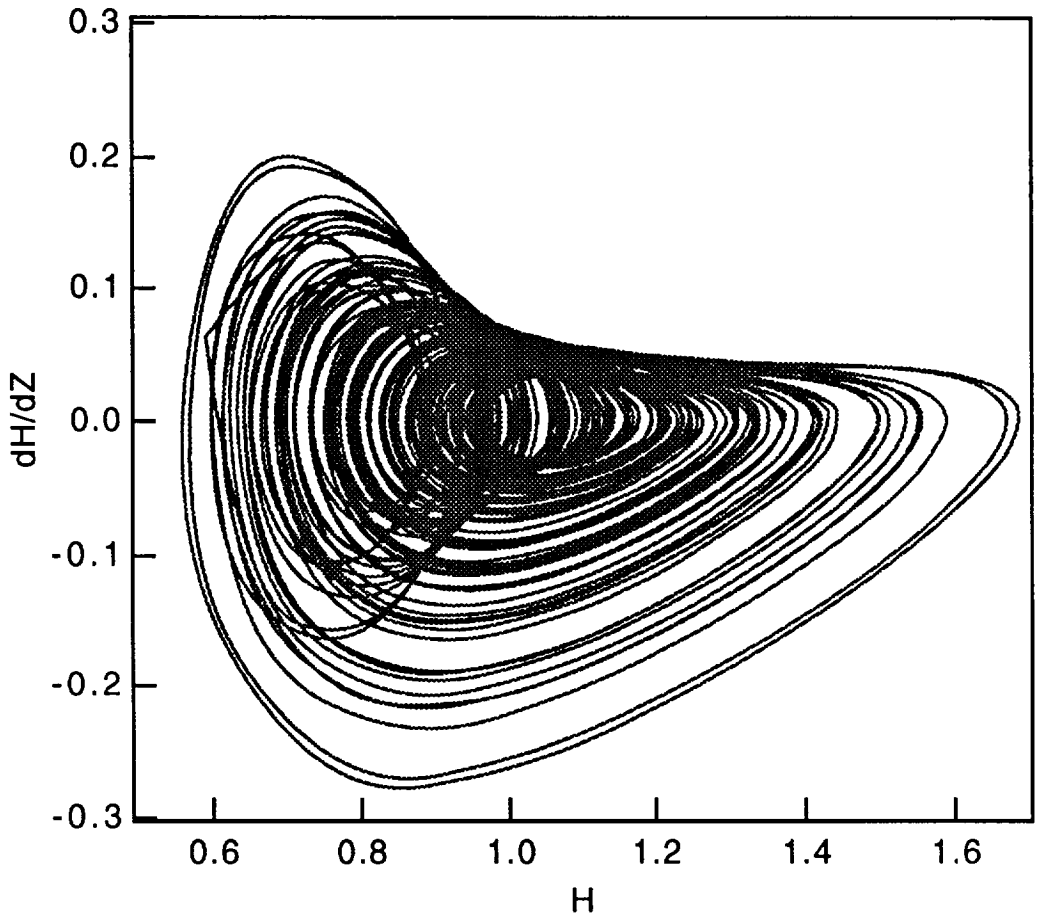

Figure 7: Film slope vs. film thickness phase plane for Re = 600, M = -0.2 and Ce = 1.785.

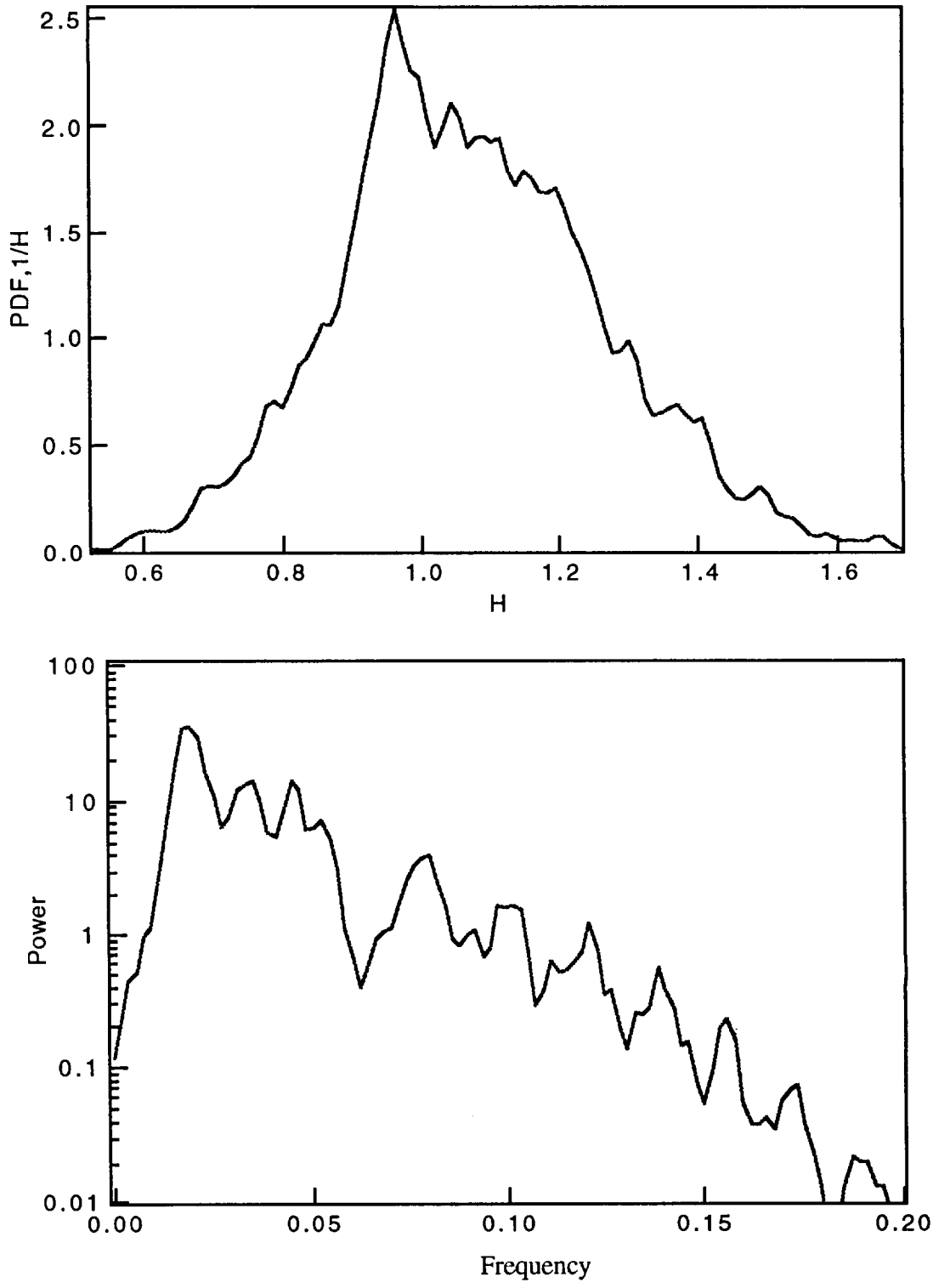

Figure 8: Normalized probability density function (top diagram) and power spectra (bottom diagram) for Re = 600, M = -0.2 and Ce = 1.785.

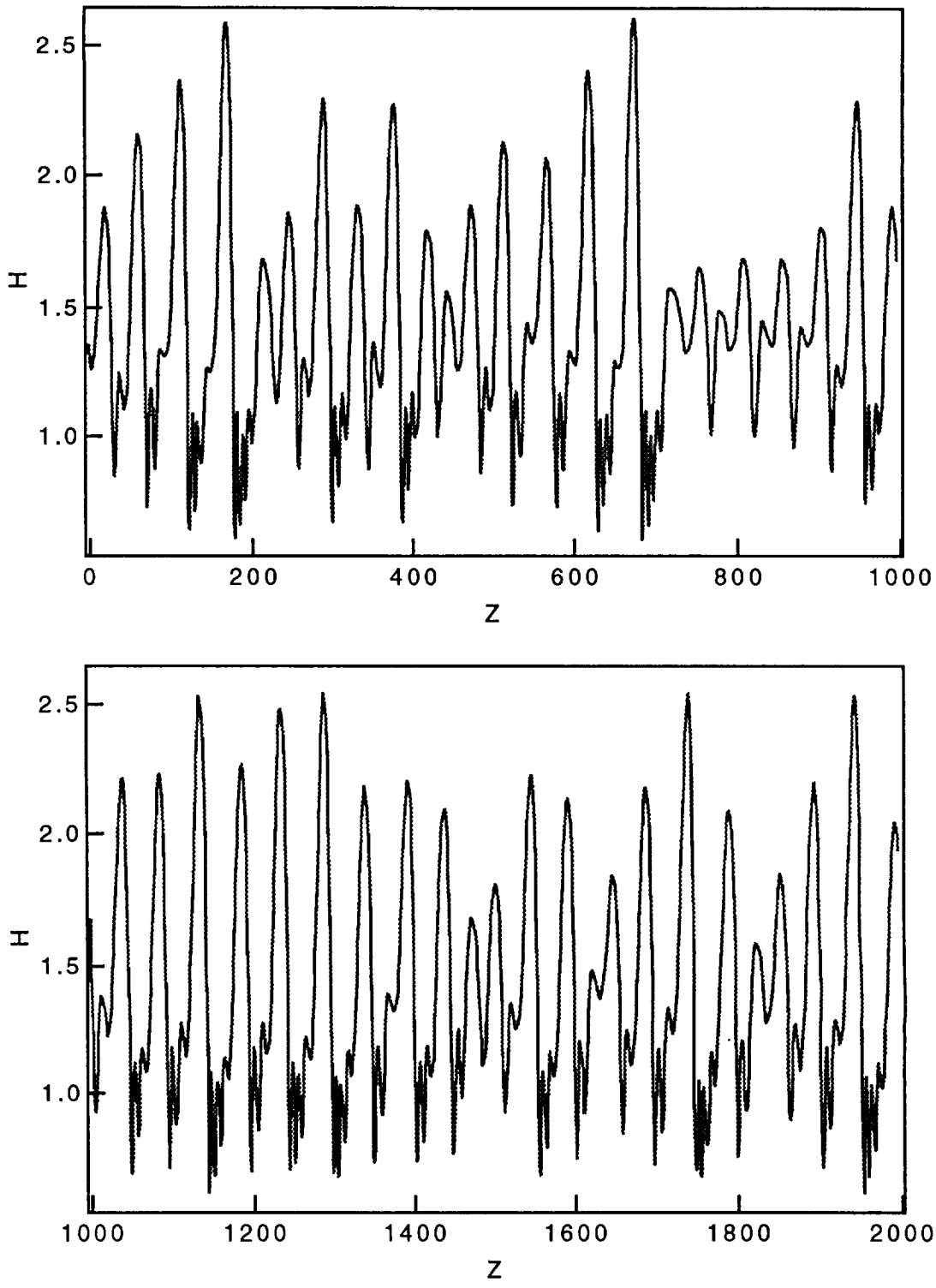

Figure 9: Film thickness profile vs. distance for Re = 600, M = -1.0 and Ce = 1.91.

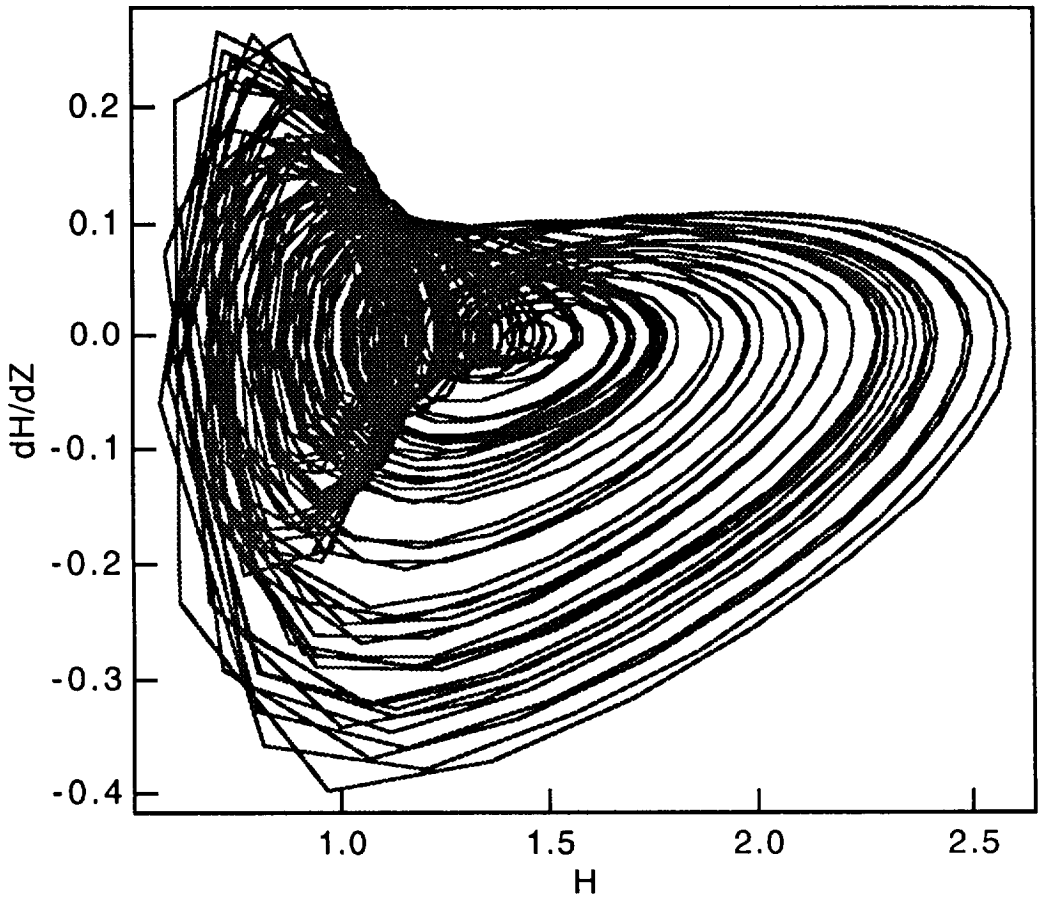

Figure10: Film slope and film thickness phase plane for Re = 600, M = -1.0 and Ce = 1.91.

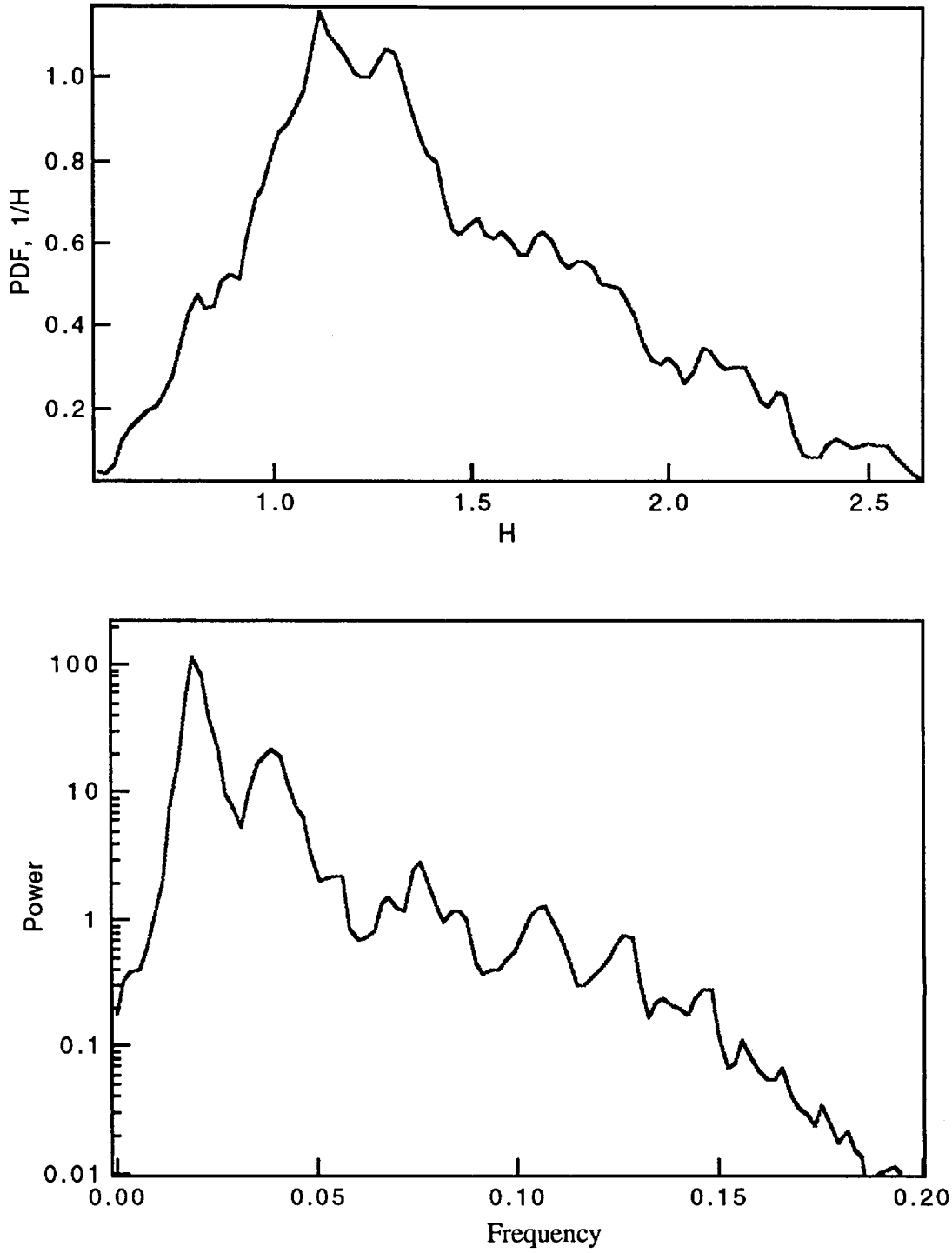

Figure 11: Normalized probability density function (top diagram) and power spectra (bottom diagram) at Re = 600, B = -1.0 and Ce = 1.91.

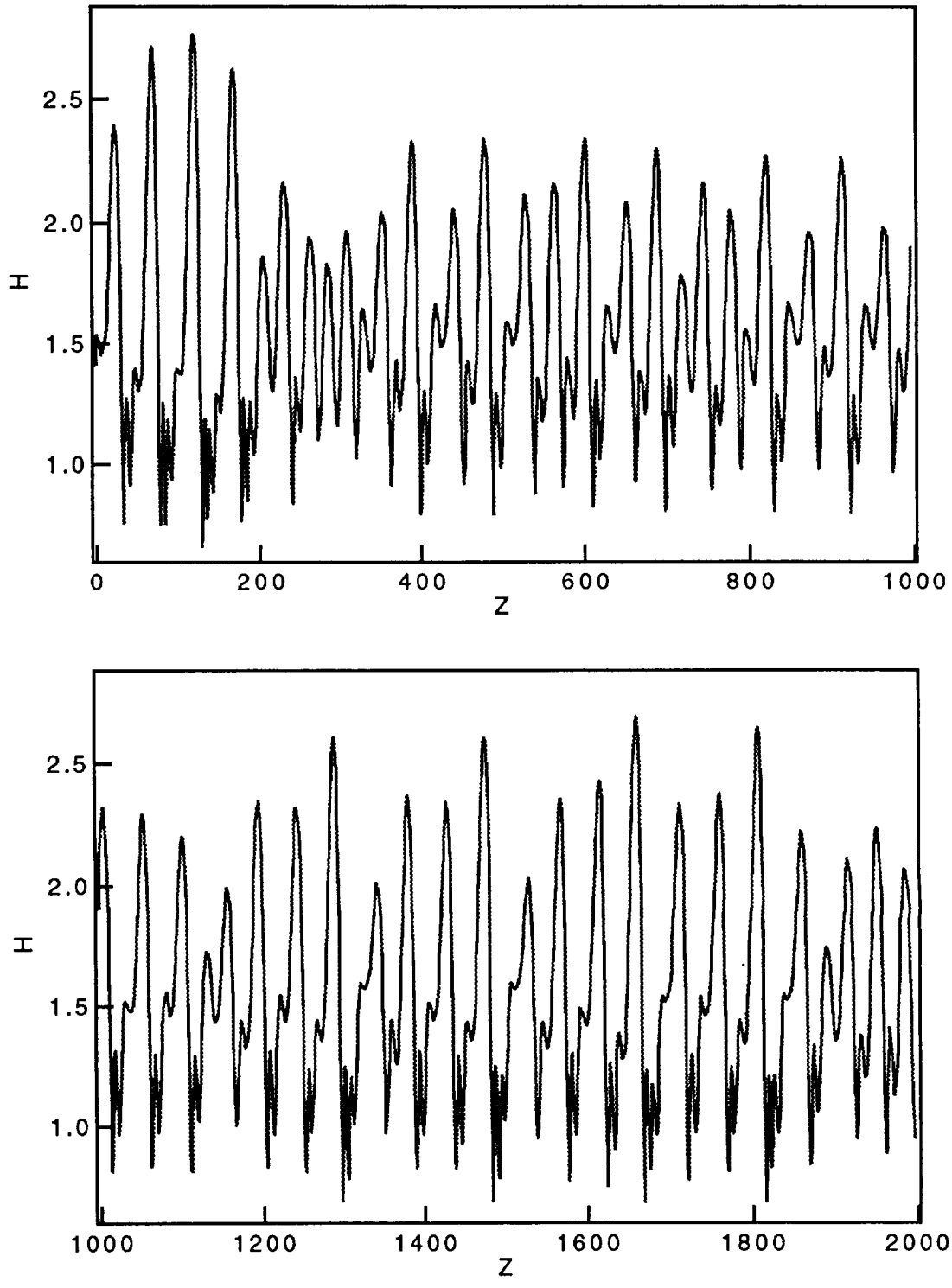

Figure 12: Film thickness profile for Re = 600, M = -1.3 and Ce = 1.97.

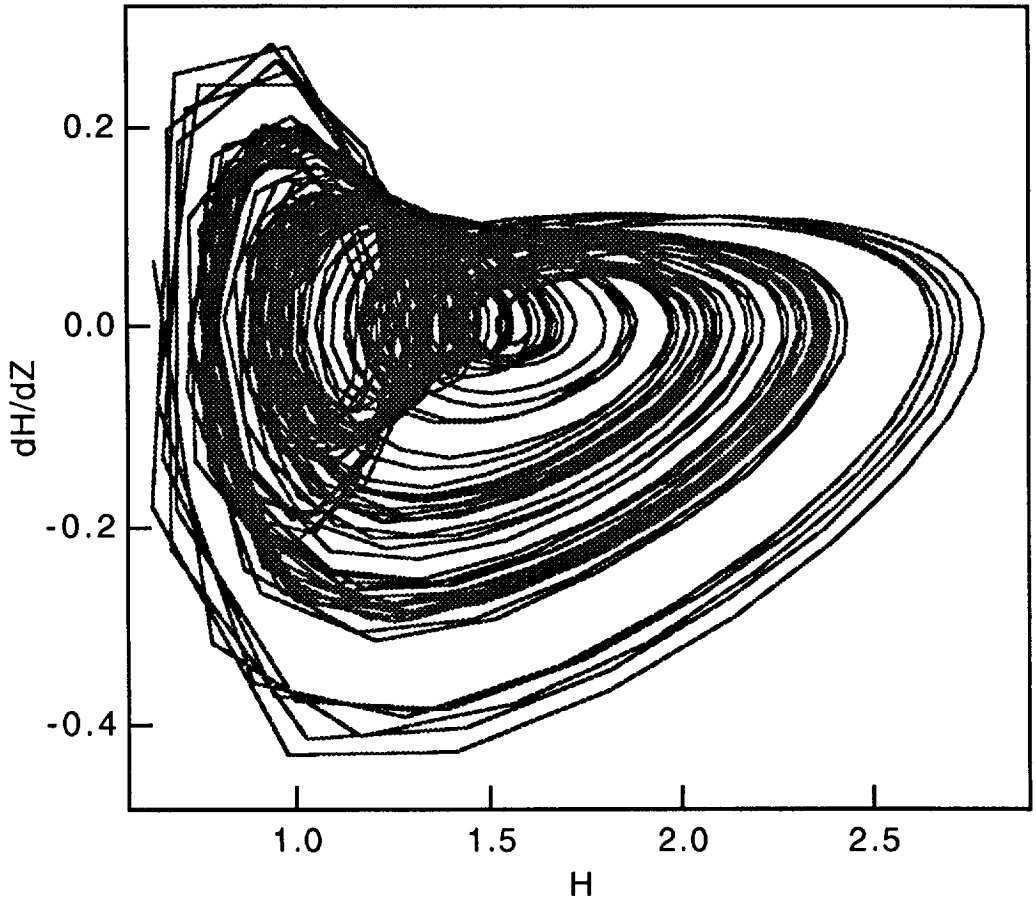

Figure 13: Film slope vs. film thickness phase plane for Re = 600, M = -1.3 and Ce = 1.97.

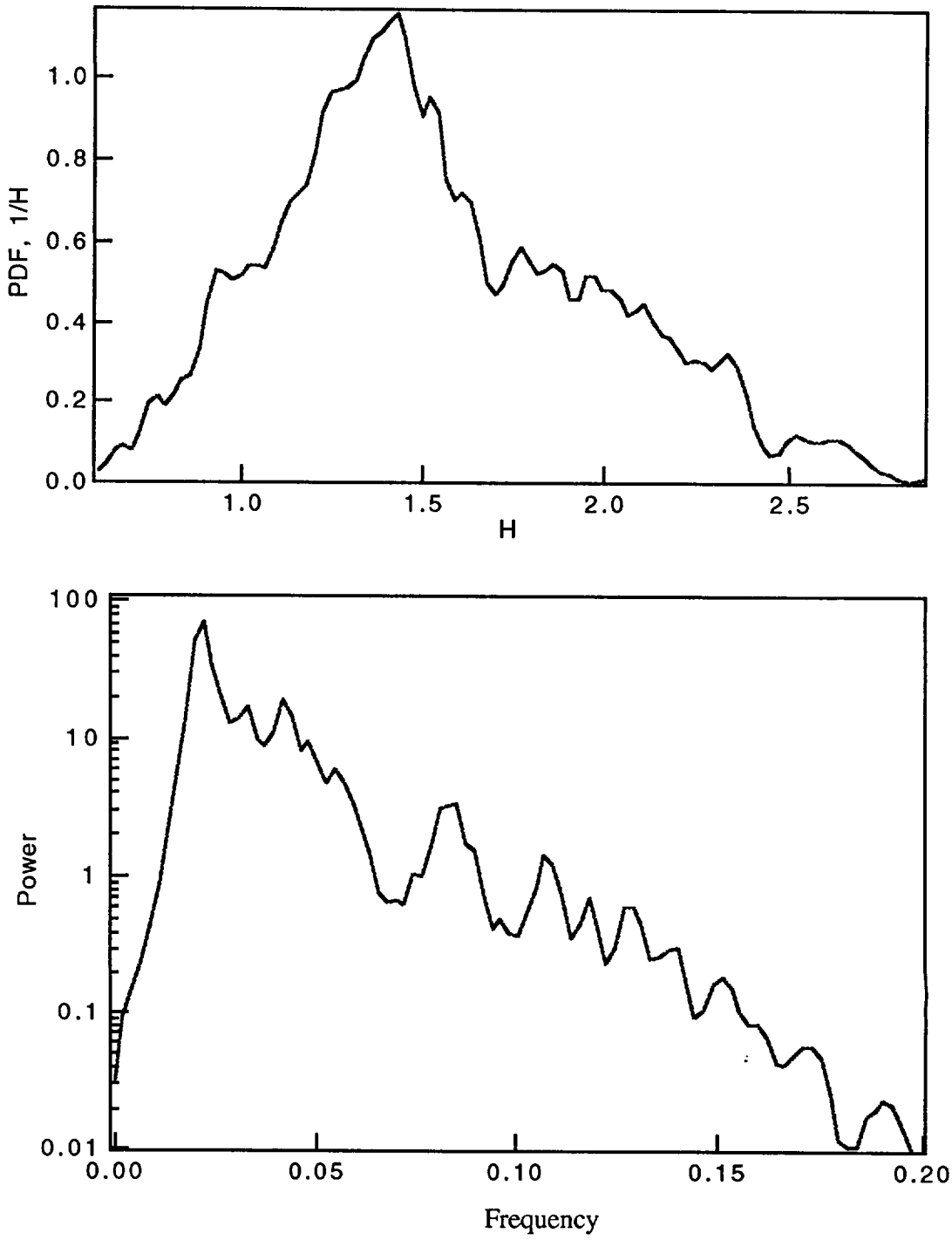

Figure 14: Normalized probability density function (top diagram) and power spectra (bottom diagram) for Re = 600, M = -1.3 and Ce = 1.97.

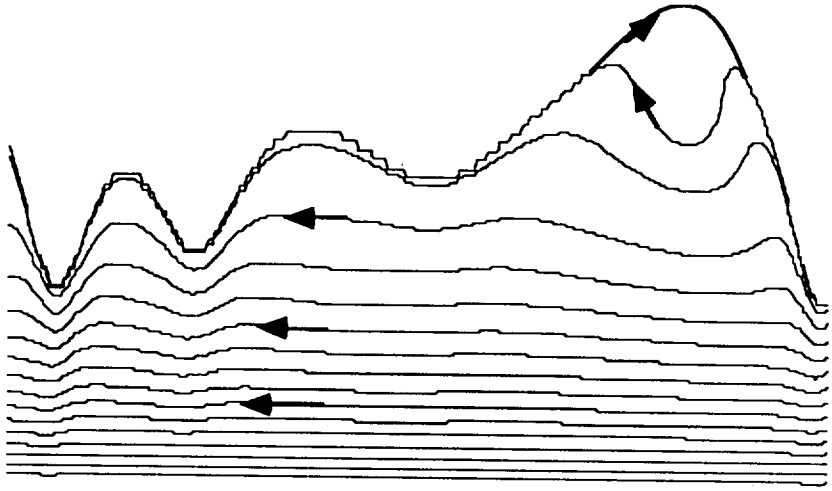

Hpeak/substrate = 2.5

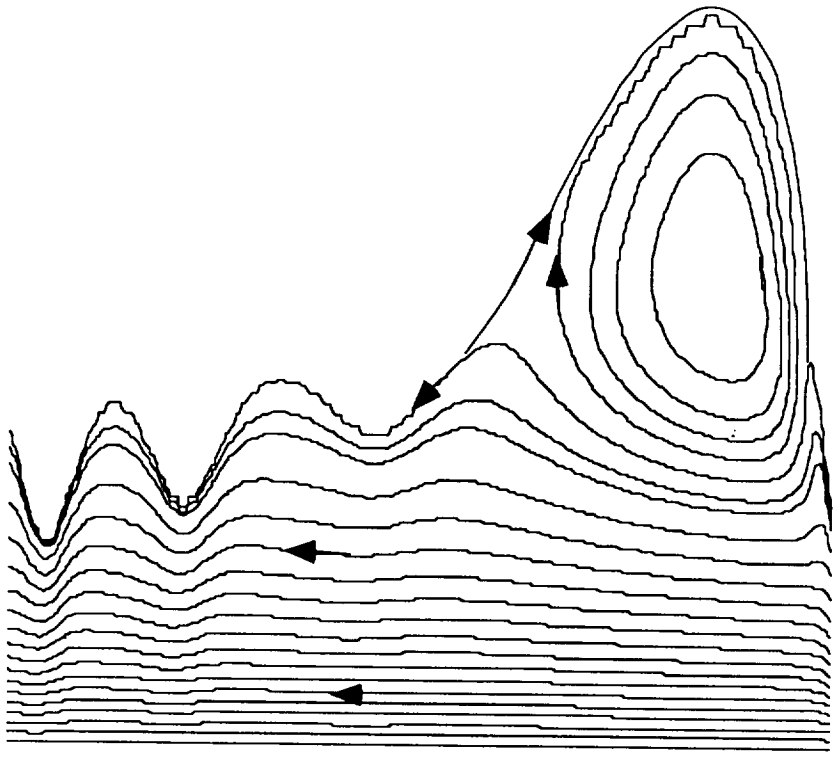

Hpeak/substrate = 3.5

Figure15: Computed streamlines under the large waves for two values of the peak thickness to substrate thickness ratio for Re = 600, M = -0.6 and Ce = 1.84.

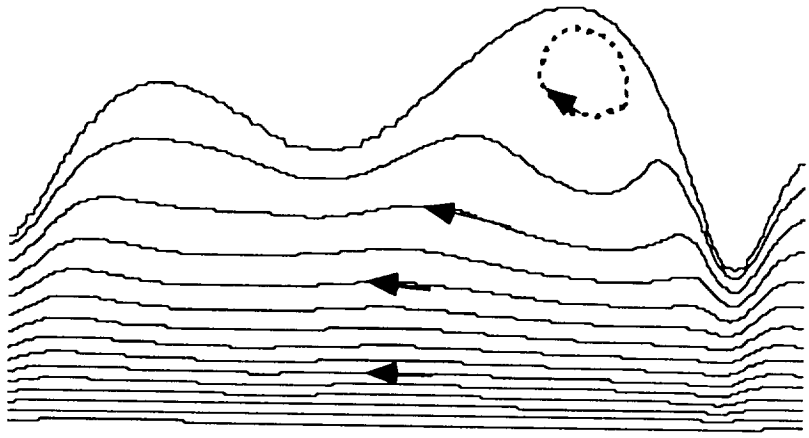

Hpeak/substrate = 2.5

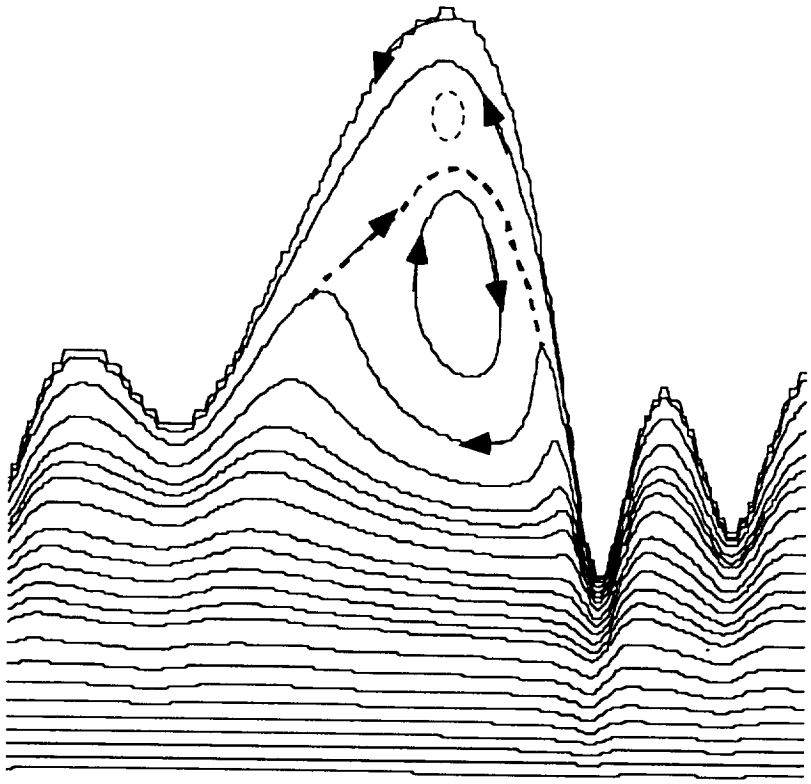

Hpeak/substrate = 5

Figure 16: Computed streamlines under the large waves for two values of the peak thickness to substrate thickness ratio for Re = 600, M = -1.0 and Ce = 1.91.

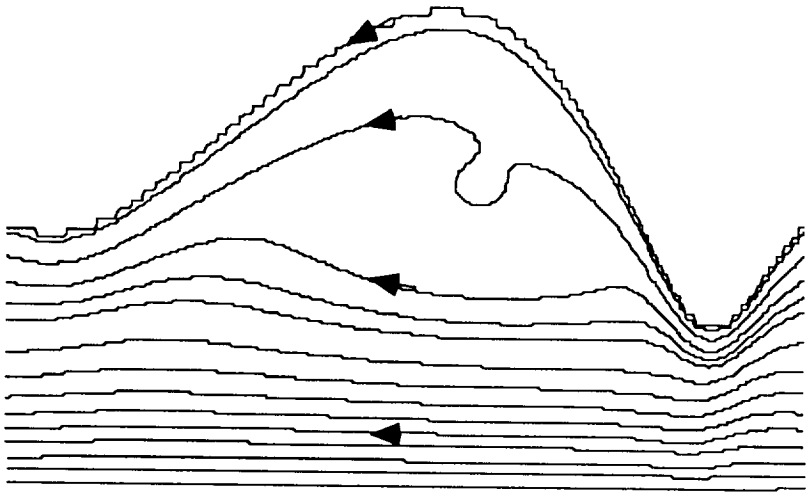

Hpeak/substrate = 2.6

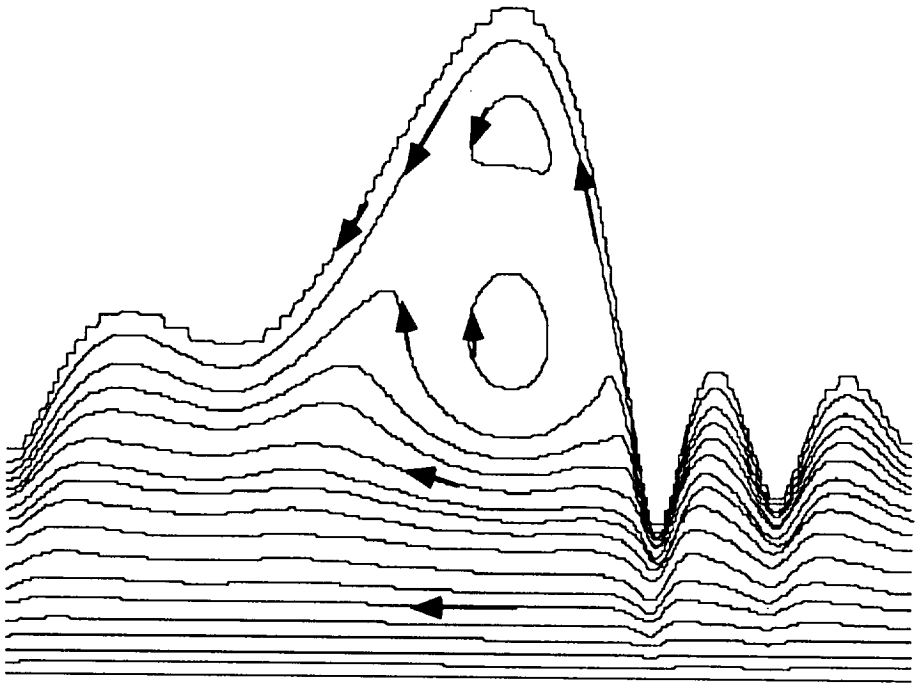

Hpeak/substrate = 6

Figure17: Computed streamlines under the two waves for two values of the peak to substrate thickness ratio. Re = 600, M = -1.3 and Ce = 1.97.